

FILE COPY

4

GL-TR-89-0123

Preliminary Investigation of Faraday Rotation
Effects and Description of Polarization
Measurements on the AFGL High Latitude Meteor
Scatter Test Bed

AD-A211 298

Jens C. Ostergaard

Elektronikcentralen
2970 Horsholm, DENMARK

1 January 1989

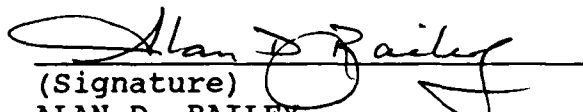
Final Report
June 1988 - May 1989

APPROVED FOR PUBLIC RELEASE; DISTRIBUTION UNLIMITED

GEOPHYSICS LABORATORY
AIR FORCE SYSTEMS COMMAND
UNITED STATES AIR FORCE
HANSCOM AIR FORCE BASE, MASSACHUSETTS 01731-5000

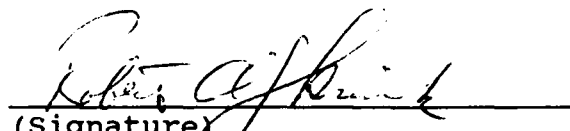
DTIC
ELECTE
AUG 14 1989
S
D
M

"This technical report has been reviewed and is approved for publication"


(Signature)
ALAN D. BAILEY
Contract Manager


(Signature)
JOHN E. RASMUSSEN
Branch Chief

FOR THE COMMANDER


(Signature)
ROBERT A. SKRIVANEK
Division Director

This report has been reviewed by the ESD Public Affairs Office (PA) and is releasable to the National Technical Information Service (NTIS).

Qualified requestors may obtain additional copies from the Defense Technical Information Center. All others should apply to the National Technical Information Service.

If your address has changed, or if you wish to be removed from the mailing list, or if the addressee is no longer employed by your organization, please notify GL/IMA, Hanscom AFB, MA 01731. This will assist us in maintaining a current mailing list.

Do not return copies of this report unless contractual obligations or notices on a specific document requires that it be returned.

REPORT DOCUMENTATION PAGE

1a REPORT SECURITY CLASSIFICATION Unclassified			1b RESTRICTIVE MARKINGS			
2a SECURITY CLASSIFICATION AUTHORITY			3 DISTRIBUTION/AVAILABILITY OF REPORT Approved for public release; Distribution unlimited.			
2b DECLASSIFICATION/DOWNGRADING SCHEDULE						
4 PERFORMING ORGANIZATION REPORT NUMBER(S)			5 MONITORING ORGANIZATION REPORT NUMBER(S) GL-TR-89-0123			
6a NAME OF PERFORMING ORGANIZATION Elektronikcentralen		6b OFFICE SYMBOL (if applicable)	7a NAME OF MONITORING ORGANIZATION Det 1, 3 Space Support Wing			
6c ADDRESS (City, State and ZIP Code) 2970 Horsholm, DENMARK			7b ADDRESS (City, State, and ZIP Code) US Embassy 2100 Copenhagen, DENMARK			
8a NAME OF FUNDING/SPONSORING ORGANIZATION Geophysics Laboratory		8b OFFICE SYMBOL (if applicable) LID	9 PROCUREMENT INSTRUMENT IDENTIFICATION NUMBER F61101-88-C-0015			
8c ADDRESS (City, State, and ZIP Code) Hanscom AFB Massachusetts 01731-5000			10 SOURCE OF FUNDING NUMBERS			
			PROGRAM ELEMENT NO 62101F	PROJECT NO 4643	TASK NO. 10	WORK UNIT ACCESSION NO. 08
11 TITLE (Include Security Classification) Preliminary Investigation of Faraday Rotation Effects and Description of Polarization Measurements on the AFGL High Latitude Meteor Scatter Test Bed						
12 PERSONAL AUTHOR(S) Jens C. Ostergaard						
13a TYPE OF REPORT Scientific Final		13b TIME COVERED FROM Jun 88 TO May 89		14 DATE OF REPORT (Year, Month, Day) 1989 January 1		15 PAGE COUNT 56
16 SUPPLEMENTARY NOTATION Prepared under scientific exchange agreement between United States Air Force and Denmark; Project 24/87 Polar Radio Propagation						
17 COSATI CODES			18 SUBJECT TERMS (Continue on reverse if necessary and identify by block number)			
FIELD	GROUP	SUB-GROUP	Meteor Scatter (MS)		Faraday Rotation	
			Propagation		High Latitude Propagation	
			Communications			
19 ABSTRACT (Continue on reverse if necessary and identify by block number) The background, methodology and preliminary results of an investigation of Faraday rotation effects on the Air Force Geophysics Laboratory Meteor Scatter High Latitude Test Bed in Greenland are presented. A short review of polarization theory for radio waves, presenting basic properties and changes when reflected from the surface of the earth or propagated through the ionosphere is included. Material published by other workers is presented to give the background for the current interest in Faraday rotation on meteor scatter links. Propagation losses for meteor scatter paths originate from spatial spreading of RF energy, scattering losses at the meteor trail, ionospheric absorption and polarization mismatch at the receiving antenna. That part of the polarization mismatch generated by the ionosphere, the Faraday rotation, is described and evaluated. A method to compute the Faraday rotation is presented and results obtained for the AFGL MSHL Test Bed are given. An experiment, including the measurement of signal strength and polarization throughout the lifetime of the individual meteor scatter return is needed to fully asses the combined affects of absorption and depolarization during both quiet and disturbed ionospheric						
20 DISTRIBUTION/AVAILABILITY OF ABSTRACT <input type="checkbox"/> UNCLASSIFIED/UNLIMITED <input type="checkbox"/> SAME AS RPT <input type="checkbox"/> DTIC USERS			21 ABSTRACT SECURITY CLASSIFICATION Unclassified			
22a NAME OF RESPONSIBLE INDIVIDUAL Alan D. Bailey			22b TELEPHONE (Include Area Code) (617) 377-2525		22c OFFICE SYMBOL GL/LID	

CONT OF BLOCK 19:

conditions. The measurement accuracy to be expected from a proposed experiment is evaluated. A few examples of meteor scatter returns obtained with a prototype experiment in Greenland are shown and discussed. ()

ACKNOWLEDGEMENTS:

The author wants to thank:

Mr. J. Rasmussen and Dr. P. Kossey, AFGL, for the opportunity and continuing encouragement to work with the subject.

Mr. A. Bailey, Mr. J. Heckscher, SMSgt A. Coriaty, MSgt D. Mura, Sgt C. Curtis, Mr. J. Borghetti, AFGL, and Mr. E. Li, ULCAR, for valuable discussions, contributions to the construction of the antennas, and for great companionship in the field.

Dr. A. Hedberg, Uppsala Ionospheric Observatory, Sweden, for providing the raytracing program and kind tutoring on its use.

Dr. P. Cannon, RAE, for valuable discussions on Faraday rotation.

Mr. W. Klemetti, and Ms D. Halacy, AFGL, for help with the manuscript and illustrations.

Accession For	
NTIS GRA&I	<input checked="" type="checkbox"/>
DTIC TAB	<input type="checkbox"/>
Unannounced	<input type="checkbox"/>
Justification	
By _____	
Distribution/	
Availability Codes	
Dist	Avail and/or Special
AI	

Contents:

1. Introduction.
2. Polarization of Radiowaves in General.
3. The Polarization of Antennas.
4. Depolarization in Meteor Scatter.
5. Depolarization of Radiowaves by Reflection From the Earth.
6. Faraday Rotation.
7. Faraday Rotation in Meteor Scatter Propagation.
8. Computation of Faraday Rotation by Raytracing.
9. Computed Faraday Rotation for Selected Ionospheric Paths.
10. Discussion of the Results.
11. Experimental Setup for Measurement of Signal Strength and Polarization.
12. Description of the Receiver.
13. Description of the Antennas.
14. Assessment of Measurement Capability and Accuracy.
15. Preliminary Measurement Results.
16. Conclusions.

List of Illustrations:

- 2.1 Illustration of orthogonal polarizations. The polarization ellipses have the same eccentricity.
- 3.1 Polarization ellipses for $p = 0.5$, with arguments between 0 and 360 deg. in increments of 20 deg.
- 4.1 Sources of depolarization on a meteor scatter link.
- 5.1 Coordinate system used to describe the general case of reflection from a plane surface. After Beckmann.
- 6.1 Illustration of the Faraday rotation mechanism for a homogeneous, collisionless layer of plasma. The wave propagates in the direction of the external magnetic field. After Beckmann.
- 9.1 Electron density profiles used for computation of Faraday rotation by raytracing. Profile A is for undisturbed ionospheric conditions. Profiles B and C are for vertical absorption of 2 dB and 7 dB respectively at 30 MHz during a Polar Cap Absorption event.
- 9.2 Collision frequency profile used for computation of Faraday rotation by raytracing.
- 9.3 Polarization ellipses computed for the path between a transmitter at Thule AB, Greenland to a midpath position towards Sondrestrom AB, Greenland.
- 9.4 Polarization ellipses computed for the path between the midpath position and a receiver at Sondrestrom AB, Greenland.
- 10.1 Height distribution of meteor trail scatterers. After Clegg, Davidson.
- 11.1 New receiving system configuration.
- 12.1 Functional schematic of the new receiver.
- 12.2 New receiver layout (top PCB).
- 13.1 Return losses for a set of 5 element crossed Yagi antennas at 104 MHz.

- 13.2 Isolation between a set of 5 element crossed Yagi antennas at 104 MHz.
- 13.3 Return losses for a set of six element crossed Yagi antennas. H and V denotes the Horizontal and Vertical antenna respectively.
- 13.4 Isolation between a set of crossed, six element Yagis at 104 MHz.
- 13.5 Polarization purity of a set of five element, 104 MHz crossed Yagis. H and V denotes the response to a linearly polarized test signal versus the angle of the transmitting antenna, of the Horizontal and the Vertical antennas, respectively.
- 14.1 Spectrum of the transmitted signal. The signal was FM modulated with a 400 Hz tone and the frequency deviation was 1 kHz.
- 14.2 Passband of the phase locked FM detector.
- 14.3 Acquisition level as a function of the noise level at the antenna port. The measurement was performed at 85 MHz using an external signal generator and a noise source.
- 14.4 Acquisition time of the receiver. The figure presents the acquisition flag as a function of the time after a -110 dBm signal was applied to the horizontal antenna input. The acquisition time is 40 milliseconds.
- 14.5 Contour plots of the error obtained when polarization data recorded with the AFGL meteor scatter receiving facility at Thule, Greenland, are interpreted with model antennas. A: Horizontally polarized dipole. B: RHC polarized antenna.
- 14.6 Amplitude transfer function of the post detector filters.
- 14.7 Examples of the measured diurnal variation of the system noise at 35 and 85 MHz at Thule.
- 15.1 Example of a five second recording with a number of short and weak meteor scatter returns.
- 15.2 Examples of five second recordings showing classical meteor scatter returns.
- 15.3 Example of a 12 second recording of sporadic-E signal. The polarization at A,B,C is shown.

List of Tables

- 3.1 The polarization efficiency for a wave with a polarization factor of 0.5 received by a RHC antenna, as a function of the argument of the wave polarization factor.
- 14.1 Means and standard deviations of 38 measurements of the amplitude and phase of the built in calibration generator. The measurements were performed over a two day period.

1. INTRODUCTION

This note describes the background, methodology and preliminary results of an investigation of Faraday rotation effects on the Air Force Geophysics Laboratory (AFGL) Meteor Scatter Test Bed between Sondrestrom AB and Thule AB, Greenland. The approximately 1200 km, South - North link is currently used to assess the performance of meteor scatter communication systems, operating between 45 MHz and 104 MHz, at high latitudes. It is of special interest to investigate the performance during Polar Cap Absorption (PCA) events, since the frequencies used for meteor scatter communication suffer less absorption than frequencies in the HF band. It is thus expected that meteor scatter communications will be more survivable during these events than HF circuits.

The note contains a short review of polarization theory for radio-waves, to recapitulate the basic properties of polarization, and polarization changes when radiowaves are reflected from the surface of the earth or propagated through the ionosphere. Propagation losses for meteor scatter paths originate from the spatial spreading of the RF energy, scattering losses at the meteor trail, ionospheric absorption and polarization mismatch at the receiving antennas. The part of the polarization mismatch generated by the ionosphere, the Faraday rotation is described and evaluated. Material published by other workers is presented to give the background for the current interest in Faraday rotation on meteor scatter links. A method to compute the Faraday rotation is described and results obtained for the AFGL Meteor Scatter Test Bed are presented.

The results indicate that an experiment, including the measurement of signal strength and polarization throughout the life time of the individual meteor scatter returns is needed to fully assess the combined effects of absorption and depolarization during quiet and disturbed ionospheric conditions. The experimental setup which will be used to enhance the AFGL Meteor Scatter Test Bed in Greenland is described, with special emphasis on the receiver and antennas. The measurement accuracy to be expected from this system is evaluated and presented.

Finally, a few examples of meteor scatter returns obtained with a prototype of the system in Greenland are shown and discussed.

2. POLARIZATION OF RADIOWAVES IN GENERAL

The polarization of a radiowave describes the orientation of the field vectors of an electromagnetic wave at a given point during one period of oscillation. In electromagnetic wave propagation, polarization refers to the direction of the electric field strength vector E .

A change of polarization by propagation, reflection, scattering, or diffraction is termed DEPOLARIZATION.

In general, radiowaves are elliptically polarized, ie. the E vector describes an either right hand or left hand rotating ellipse perpendicular to the direction of propagation. The commonly used polarizations in communication systems are special cases of elliptical polarization. Linear polarization is obtained if one axis of the ellipse is zero. The E vector will then describe a straight line perpendicular to the direction of propagation. Horizontal polarization and vertical polarization refer to linear polarizations for which the direction of the E vector is parallel or perpendicular to the horizon, referenced to the earths surface. The terms horizontal and vertical polarization have no meaning in space where the horizon as a reference does not exist. Circular polarization is obtained if the axis of the ellipse have equal lengths. The E vector then describes a circle perpendicular to the direction of propagation. Depending on the direction of rotation, the polarization is termed: Right Hand Circular (RHC), or Left Hand Circular (LHC). RHC is defined as the polarization turning clockwise seen from behind, ie. looking in the direction of propagation.

Two polarizations are orthogonal if: $E_1 \cdot E_2^* = 0$. Orthogonally polarized waves are in general counterrotating elliptically polarized waves with equal eccentricity, and with their major axis perpendicular to each other, Figure 2.1. In particular, horizontal and vertical polarizations are orthogonal, as are RHC and LHC polarizations.

The polarization of a radiowave can be described by the complex polarization factor P. For a wave composed from two orthogonal linear polarized waves, ie. vertical and horizontal, P can be expressed as:

$$P = \frac{E_+}{E_-} = \left| \frac{E_+}{E_-} \right| \exp(i \text{ARG}(E_+) - i \text{ARG}(E_-)) = \left| \frac{E_+}{E_-} \right| \exp(i\theta)$$

Where E_+ is the amplitude of the vertically polarized wave, E_- is the amplitude of the horizontally polarized wave, and θ is the phase difference between the waves. The polarization factor P is a convenient measure of the polarization of a radiowave, and the

resulting polarization P2 of a wave, with an initial polarization P1, after being depolarized by some process such as reflection or Faraday rotation is obtained as:

$$P2 = A P1$$

where A is a complex function descriptive of the depolarizing process.

Any polarization can be obtained by superposition of two orthogonal polarizations having different amplitudes and phases, and for any polarization, an orthogonal polarization exists. Thus, any linear polarization can be obtained from a vertically polarized and a horizontally polarized wave with different amplitudes, but equal phases, and circular polarizations are obtained from two orthogonal, linearly polarized waves with equal amplitudes and a 90 deg. phase difference. The direction of rotation is determined by the sign of the phase difference. Also, any linear polarization can be obtained from two LHC and RHC polarized waves with equal amplitudes and proper phase differences. If the amplitudes are not equal, elliptical polarization is obtained.

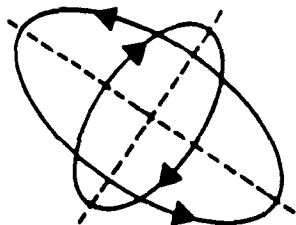


Figure 2.1. Illustration of orthogonal polarizations. The polarization ellipses have the same eccentricity.

3. THE POLARIZATION OF ANTENNAS

The polarization of an antenna is defined as the polarization of the wave radiated from the antenna, when used for transmitting. This antenna polarization is also optimal for reception of the radiated wave. An antenna with a orthogonal polarization is 'blind' to the radiated wave, when used for reception. This is well known for the cases of linear and circular polarizations. A vertically polarized antenna is blind to horizontally polarized waves, and a RHC polarized antenna cannot receive LHC polarized waves, but the concept applies generally to any elliptical polarization.

The gain of an antenna is defined for its specific polarization, and waves with other polarizations will be received with less efficiency than waves which have the same polarization as the antenna. The decrease in reception efficiency is termed POLARIZATION MISMATCH, or POLARIZATION DISCRIMINATION. Thus, a linearly polarized antenna will exhibit 3 dB less gain than a comparable circularly polarized antenna when used for reception of circularly polarized waves, whereas a pair of orthogonal linearly polarized antennas with the proper phasing can be matched to the polarization of the wave, so no polarization mismatch occurs.

The degree of mismatch can be expressed as the polarization efficiency, defined as the ratio of the power delivered to a matched load by the antenna to the maximum power obtainable with a polarization matched antenna:

$$n = |1 + pt^*|^2 / (1 + |t|^2)(1 + |p|^2)$$

where n is the polarization efficiency, t is the polarization of the antenna, and p is the polarization of the received wave.

As an example, consider a horizontally polarized wave being received by a RHC polarized antenna. The polarization factor of the wave is 0, and the polarization of the antenna is 'i'. The formula yields:

$$n = |1 + 0i|^2 / (1 + |0+i|^2)(1 + |0|^2) = 0.5$$

Thus, half of the maximum power is obtained. If a RHC wave with the polarization 'i' was used, then $n = 1$. The antenna is matched to the wave.

The polarization of the antennas used in communication systems are most often simple linearly or circularly polarized antennas, whereas the waves to be received can be arbitrarily polarized. It is therefore of interest to examine the polarization mismatch between simple antennas and randomly polarized waves.

Consider a horizontal and a vertical dipole antenna, which both receive a wave with the polarization factor 0.3, for which the argument varies. Fig. 3.1. shows the polarization ellipses for waves with arguments of the polarization factor between 0 and 360 deg. in increments of 20 deg. It is seen that the projection of the ellipses on the horizontal and vertical axis are independent of the argument. Thus the power received by the two antennas is also independent of the argument.

However, if the same wave was received with a RHC antenna, then the argument 90 deg yields $n = 0.9$, whereas the argument -90 deg. yields $n = 0.1$. The argument is very important in this case. Table 3.1 presents the polarization efficiency as a function of the argument for this special case.

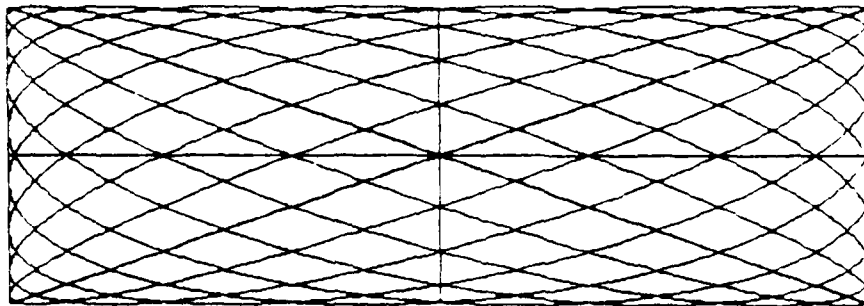


Fig. 3.1. Polarization ellipses for $p = 0.3$, with arguments between 0 and 360 deg. in increments of 20 deg.

0deg.	$n=0.900$
10deg.	$n=0.894$
20deg.	$n=0.876$
30deg.	$n=0.846$
40deg.	$n=0.806$
50deg.	$n=0.757$
60deg.	$n=0.700$
70deg.	$n=0.637$
80deg.	$n=0.569$
90deg.	$n=0.500$
100deg.	$n=0.431$
110deg.	$n=0.363$
120deg.	$n=0.300$
130deg.	$n=0.243$
140deg.	$n=0.194$
150deg.	$n=0.154$
160deg.	$n=0.124$
170deg.	$n=0.106$
180deg.	$n=0.100$

Table 3.1. The polarization efficiency for a wave with a polarization factor of 0.3 received by a RHC antenna, as a function of the argument of the wave polarization factor.

4. DEPOLARIZATION IN METEOR SCATTER PROPAGATION

Meteor scatter links generally use horizontally polarized transmitting antennas for fixed circuits, and in a few cases vertically polarized transmitting antennas for mobile circuits. Depolarization of the transmitted wave occurs at several places on the propagation path between the transmitter and the receiver. With reference to Figure 4.1, the earth below the transmitting antenna will reflect a part of the RF energy radiated at negative elevation angles. The resulting wave in the far field is a super-position of the direct and the reflected wave. The polarization of this wave is not necessarily the same as the polarization of the transmitting antenna. Depolarization may occur due to the influence of the ionosphere on the path between the transmitting antenna and the meteor trail. The scattering process at the meteor trail may introduce either depolarization or polarization mismatch. The scattered wave may be depolarized by the ionosphere when propagated between the meteor trail and the receiving antenna, and finally, the earth below the receiving antenna will reflect a part of the wave into the antenna aperture where it will be superimposed with the direct ray. This will create yet another depolarization.

An analytical description of the total depolarization throughout the propagation path is very involved except for a few simple cases. In general, each contribution must be considered separately and numerical methods must be used.

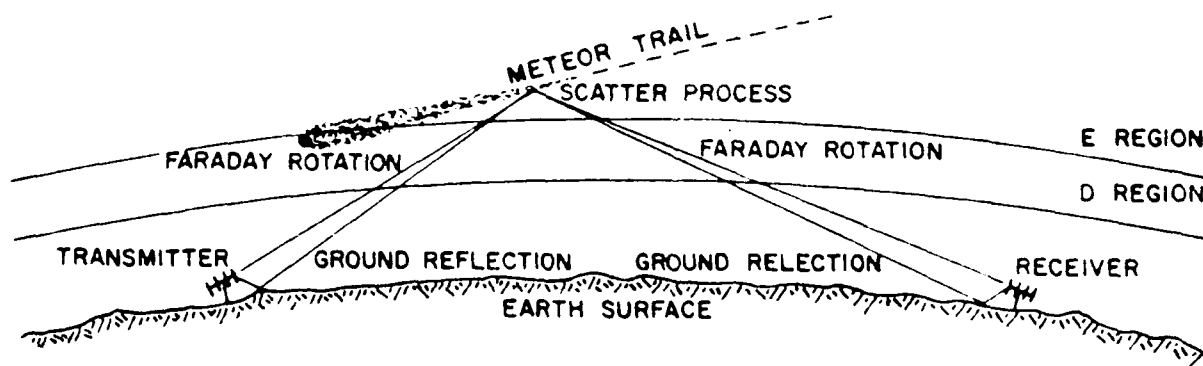


Figure 4.1. Sources of depolarization on a meteor scatter link.

5. DEPOLARIZATION OF RADIO WAVES BY REFLECTION FROM THE EARTH

The expressions for the depolarization of plane waves from the surface of the earth are only simple, if the polarization plane is parallel with, or perpendicular to, the reflecting plane. In this case, the complex reflection coefficients are determined from the Fresnel coefficient formulas:

For horizontal polarization:

$$P_h = \frac{\cos \theta - \sqrt{\epsilon' - \sin^2 \theta}}{\cos \theta + \sqrt{\epsilon' - \sin^2 \theta}}$$

For vertical polarization:

$$P_v = \frac{\epsilon' \cos \theta - \sqrt{\epsilon' - \sin^2 \theta}}{\epsilon' \cos \theta + \sqrt{\epsilon' - \sin^2 \theta}}$$

Where: $\epsilon' = \epsilon_r + i60\lambda\sigma$

θ is the angle of incidence on the reflecting surface, λ the wavelength, ϵ_r the relative dielectric constant of the reflecting surface and σ the conductivity of the reflecting surface.

The reflected waves are still linearly polarized, but the magnitude and phase of the waves have been changed according to multiplication with the Fresnel coefficients. Waves resulting from superposition of direct rays and reflected rays will be linearly polarized, with unchanged polarization, but a cancelling effect occurs when the direct and reflected rays arrive at the receiving antenna with equal magnitude and opposite phases.

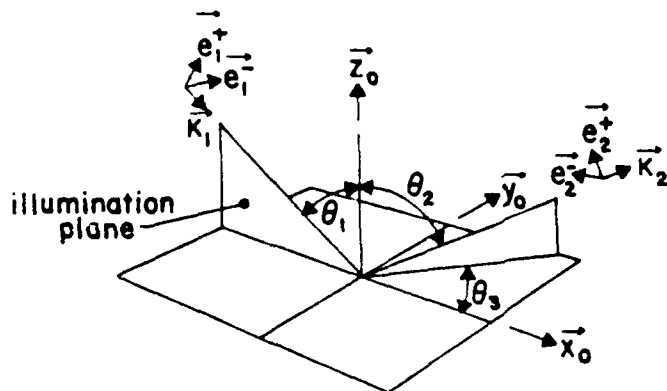


Figure 5.1. Coordinate system used to describe the general case of reflection from a plane surface. After Beckmann. (1)

With reference to Figure 5.1., the general expression for the depolarization of a plane wave with arbitrary polarization from a plane surface of arbitrary orientation is:

$$P_2 = \frac{P_1(R_v \tan \beta_1 \tan \beta_2 + R_h) + R_h \tan \beta_1 - P_v \tan \beta_2}{R_v \tan \beta_1 \tan \beta_2 + R_h + P_1(R_v \tan \beta_2 - R_h \tan \beta_1)}$$

Where:

R_h and R_v are the Fresnel coefficients, and

$$\sin \beta_1 = \sin \theta_2 \sin \theta_3 / \sin X$$

$$\sin \beta_2 = \sin \theta_1 \sin \theta_3 / \sin X$$

$$\cos X = \cos \theta_1 \cos \theta_2 - \sin \theta_1 \sin \theta_2 \cos \theta_3$$

P_2 is the polarization of the reflected wave, P_1 is the polarization of the incoming wave. An example for a selected, simple case can illustrate the properties of the formula: For a perfectly conducting plane surface, tilted around the Y-axis, the case of interest for meteor scatter systems, for which the ground in front of the antennas is near horizontal and flat, $\theta_3 = 0$, β_1 and $\beta_2 = 0$; and the formula simplifies to:

$$P_2 = (R_v / R_h) P_1$$

A special case occurs if the reflecting plane is perfectly conducting. Then $R_v = 1$, and $R_h = -1$, so that: $P_2 = -P_1$. Under this condition, a circularly polarized wave will be reflected into a circularly polarized wave of opposite sense of rotation. If the receiving antenna is polarized to match the direct ray, it will be blind to the ground reflected ray.

Linearly polarized waves will be reflected into waves with unchanged polarization, ie. a horizontally polarized wave will still be horizontally polarized after being reflected from the ground. For this reason, the antennas in horizontally polarized meteor scatter systems with ranges of approximately 1000 - 1400 km are often placed approximately 1.5 wavelengths above the ground. This position creates a maximum of 6 dB enhancement of the antenna gain at a elevation angle of approximately 10 to 14 degrees, due to constructive interference between the direct and the ground reflected waves, without a change of polarization. The elevation interval from 10 to 14 degrees is very important as this illuminates the hot spots associated with a 1000 - 1400 km link.

A similar system using circular polarization would generate an elliptically polarized far field wave, for which the excentricity-

city and the angle of the major axis will change with the elevation angle, and no gain advantage will be obtained for a circularly polarized receiving antenna. On the other hand, a circularly polarized receiving antenna will be able to provide some multipath discrimination in situations where interference between a direct and a reflected ray of approximately equal amplitude creates intersymbol interference. If the reflected ray is reflected from a perfectly conducting surface, its polarization will be counter rotating, and it will not be seen by the antenna.

6. FARADAY ROTATION

The ionosphere is an anisotropic medium, due to the presence of the earth's magnetic field. One or more parameters of such a medium change with the direction in which it is measured. One such parameter for the ionosphere is the index of refraction, n which is determined from the Appleton formula:

$$n^2 = 1 - X / (1 - iZ - \frac{Y_T^2}{2(1 - X - iZ)} \pm \sqrt{\frac{Y_T^4}{4(1 - X - iZ)^2} + Y_L^2})$$

$$X = \omega_0^2 / \omega^2, \quad Y_L = \omega_H \cos \theta, \quad Y_T = \omega_H \sin \theta, \quad Z = \nu / \omega$$

$$\omega_0^2 = Ne^2 / m\epsilon_0, \quad \omega_H = H |e| \mu_0 / m$$

Where: ω is the wave angular frequency, e is the electron charge, m is the electron mass, ν is the collision frequency in the plasma, and H is the magnitude of the earth's magnetic field. μ_0 and ϵ_0 are the magnetic permeability and electrical permittivity of free space.

A complete derivation and discussion of the properties of the Appleton formula can be found in the literature: eg. Ratcliffe⁽⁴⁾, Davies⁽³⁾, Budden⁽²⁾.

Two solutions exist to the Appleton formula, if the magnetic field is non-zero. The effect of this is the ionosphere is doubly refracting, and the polarization of a wave propagating through the ionosphere is the superposition of the polarization of two characteristic waves, the ordinary and the extraordinary wave, which propagate corresponding to the two values of the refracting index. The effect is illustrated in Figure 6.1.

Consider as an example, a layer of ionospheric plasma with a constant electron density and no collisions, and a linearly polarized wave which propagates along the magnetic field. The characteristic waves will be circularly polarized with opposite senses of rotation. The phase velocity of the two characteristic waves will differ; one will be retarded with respect to the other.

The polarization plane of the linearly polarized wave, resulting from the superposition of the two characteristic waves, will rotate along the path through the plasma. The effect is called Faraday rotation. The total Faraday rotation, F of a linearly polarized wave traversing the ionosphere can be expressed as:

$$F = \frac{2.36 \times 10^4}{f^2} H \cos \chi N \sec \phi, \quad \text{Radians}$$

Where: $2\pi f$ is the wave angular frequency, H is the magnitude of the magnetic field, χ is the angle between the magnetic field vector and the direction of propagation, N is the total electron content integrated along the propagation path, and ϕ is the angle between the direction of propagation and zenith.

If the plasma has losses, ie. the electron density and the collision frequency are high enough, the characteristic waves will be absorbed along the path. The amount of absorption will be different for the two waves, and the polarization of the wave resulting from the superposition of the two characteristic waves is elliptical.

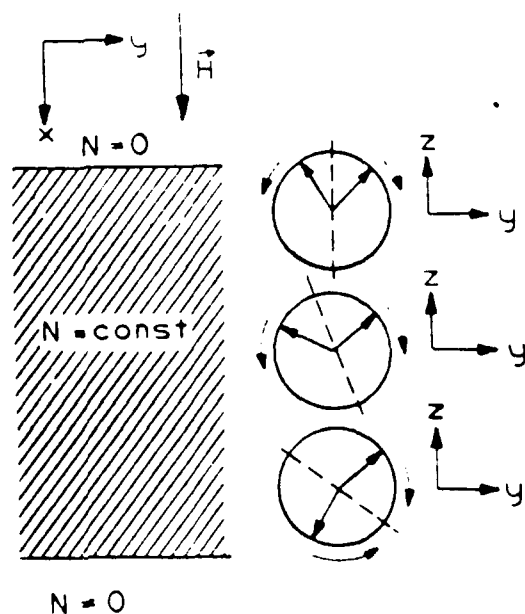


Figure 6.1. Illustration of the Faraday rotation mechanism for a homogeneous, collisionless layer of plasma. The wave propagates in the direction of the external magnetic field. After Beckmann. 1,

7. FARADAY ROTATION IN METEOR SCATTER PROPAGATION

The issue of the influence of Faraday rotation on the path-loss for a meteor scatter link has recently been raised by Cannon⁽⁹⁾, Nes⁽¹⁰⁾, and others. The effects of Faraday rotation will create polarization mismatch between the scattered wave and the receiving antenna. If this mismatch is severe enough it will impair the throughput of the link.

Two situations have been analyzed by Cannon. One is the extra pathloss due to Faraday rotation for meteor scatter links versus frequency of operation and distance, during undisturbed ionospheric conditions in Europe. The other is the extra pathloss due to Faraday rotation for a high latitude meteor scatter link during weak PCA events.

For the case of the undisturbed ionosphere, computations by Cannon⁽⁹⁾, have shown that a Faraday rotation of 90 deg. can result at 45 MHz for a link distance of 1200 km. This would create a severe polarization mismatch between the scattered wave and the receiving antenna, and a higher frequency, which suffers less Faraday rotation, would be preferable for this distance if antenna polarization matching cannot be used to counter the effect.

PCA absorption is caused by an increase of the electron density in the D and lower E-region of the ionosphere where the collision frequency is high. The increased electron density will also create additional Faraday rotation, which will introduce polarization mismatches. At 45 MHz computations presented by Cannon⁽⁹⁾ show that the losses suffered by Faraday rotation are comparable with the absorptive losses during weak PCA's. Thus higher frequencies of operation should be chosen not only to achieve less absorption, but also less polarization mismatch due to Faraday rotation.

The computations presented by Cannon⁽⁹⁾, are based on the simple formula for Faraday rotation, which is not strictly applicable if absorption is present, and the computations do not evaluate the amount of Faraday rotation obtained for the individual trail returns as a function of their altitude above the ground.

Nes⁽¹⁰⁾, has presented results of polarization measurements at 42 MHz on a path between southern Norway and the Netherlands during undisturbed ionospheric conditions. His results show for this particular case, the polarization of returns from underdense meteor trails retain their polarization, with Faraday rotations less than 20 degrees, which will not create any significant polarization mismatch. Also, he noted that the polarization of

the long lasting overdense trails started out equal to the transmitted polarization, but by the end of the trail the polarization was generally elliptical. This could possibly be due to depolarization originating from the superposition of scattered waves from different parts of a warped meteor trail.

In an effort to analyze the above mentioned computations and observations in more detail, the following paragraphs present preliminary investigations of the depolarization created by the ionosphere for the AFGL high latitude meteor scatter link in Greenland.

8. COMPUTATION OF FARADAY ROTATION BY RAYTRACING

The ionospheric depolarization can be computed by raytracing if the electron density profile between the transmitter and the point of observation of the polarization is known. A raytracing program can trace the amplitude, polarization and phase path of the ordinary and extraordinary waves through the ionosphere. Raytraces, which connect the transmitter and the point of observation, ie. the position of the meteor trail, for both characteristic waves are computed. The phase paths and the amplitudes of the waves are then combined to describe the amplitude and polarization of the wave propagated from the transmitter.

A double precision version of the NBS raytracing program (Jones, 1966)⁽⁵⁾, modified by the Uppsala Ionospheric Observatory, Uppsala, Sweden (Hamberg⁽⁶⁾, Ajayi⁽⁷⁾), was used on a IBM PC computer to compute the depolarization of a horizontally polarized wave between the earth and the position of a postulated meteor trail. First the phase path, geometric slant range and absorption were computed for the ordinary ray, for an elevation suitable to connect the chosen points on the ground and in space. Very little raybending takes place in the lower ionosphere at VHF frequencies, but the ordinary and extraordinary rays joining the two points, still do not leave the transmitter at the same elevation. Consequently, extraordinary rays were iteratively traced at different elevations until the difference in geometric slant range was less than 10 cm. The iterations were performed manually by repeated runs of the program. The polarization ellipse was then plotted for analysis of polarization mismatch. This procedure has proven to be very time consuming, and an automatic elevation homing feature must be included in the program before it is used for more involved depolarization computations.

9. COMPUTED FARADAY ROTATION FOR SELECTED IONOSPHERIC PATHS

The ionospheric depolarization has been computed with the above described raytracing program for a postulated meteor scatter path between Thule AB and Sondrestrom AB, Greenland, for which the meteor trail is positioned at the midpath on the great circle line joining the stations. Computations have been performed at 45, 65, and 104 MHz for trail heights of 80, 100 and 120 km, the range in which the meteor trails occur.

The computations are based on electron density profiles obtained with the AFGL oblique VLF/LF ionosounder at Thule. Three profiles, which are obtained under undisturbed ionospheric conditions, and during 2 dB and 7 dB ionospheric absorption conditions at 30 MHz, have been used. The profiles are presented in Figure 9.1. The collision frequency profile used for the computations is presented in Figure 9.2.

The polarization ellipses obtained from the computations for the path from a transmitter at Thule AB to the path midpoint are presented in Figure 9.3., and the polarization ellipses for the path from the meteor trail to a receiver at Sondrestrom AB are presented in Figure 9.4. The polarization ellipses represent only the ionospheric depolarization; the Faraday rotation of a horizontally polarized wave. The influence of the antennas and the foreground in front of the antennas are not included. Each polarization ellipse represents conditions at a particular frequency and postulated meteor trail height. Three sets of polarization ellipses are presented for each path. These represent results for undisturbed ionospheric conditions, 2 dB vertical absorption at 30 MHz and 7 dB vertical absorption at 30 MHz during a PCA. Each polarization ellipse is marked with two numbers, A and P. A represents the ionospheric absorption in dB if a polarization matched antenna was used to receive the signal, and P represents the polarization mismatch, in dB, to be added to A if a horizontally polarized antenna were to be used for the reception. It

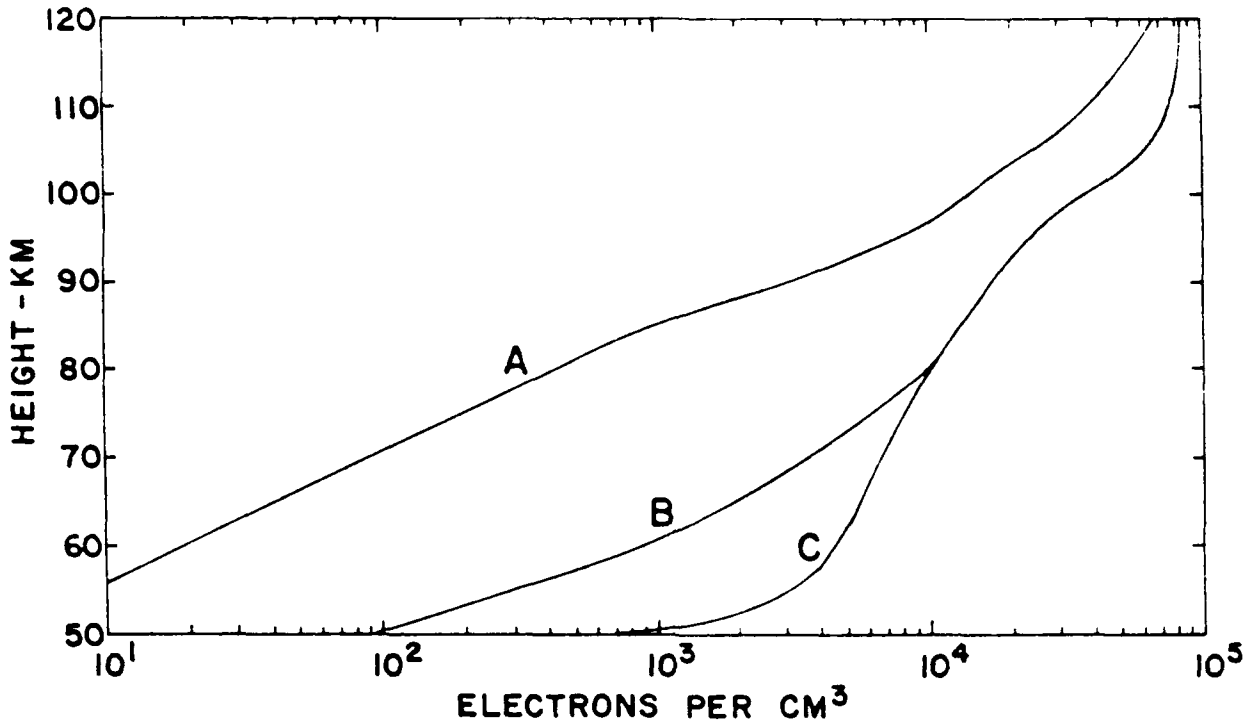


Figure 9.1. Electron density profiles used for computation of Faraday rotation by raytracing. Profile A is for undisturbed ionospheric conditions. Profiles B and C are for vertical absorption of 2 dB and 7 dB respectively at 30 MHz during a Polar Cap Absorption event.

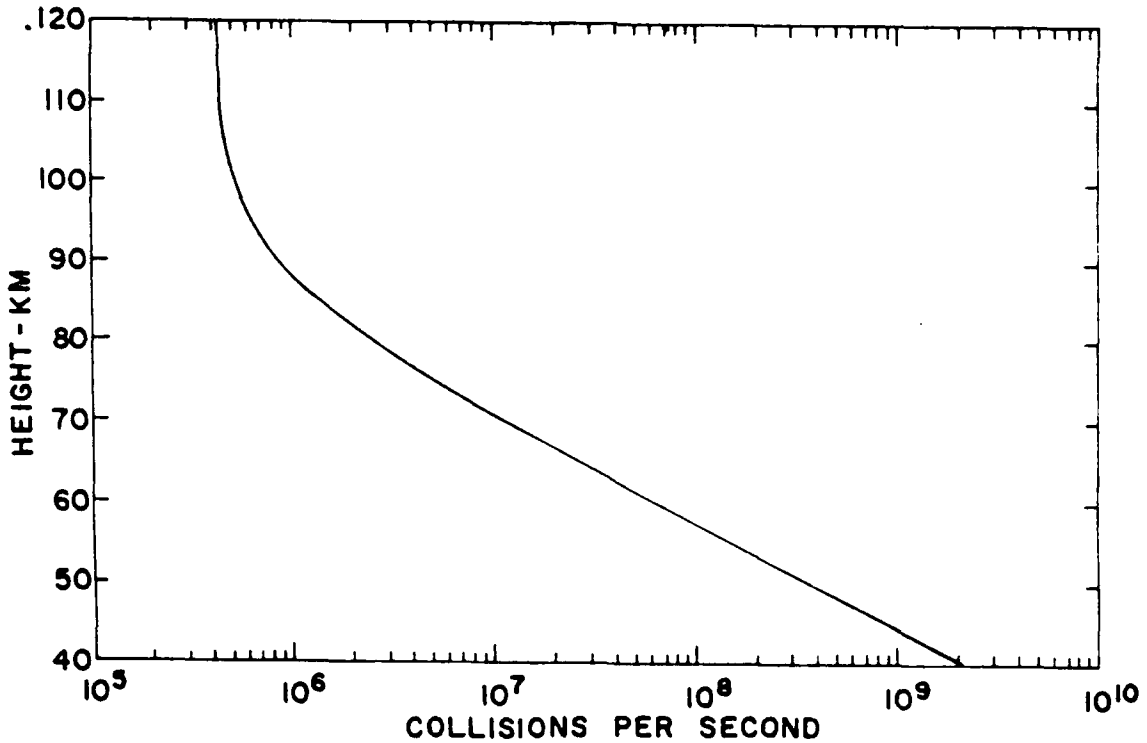
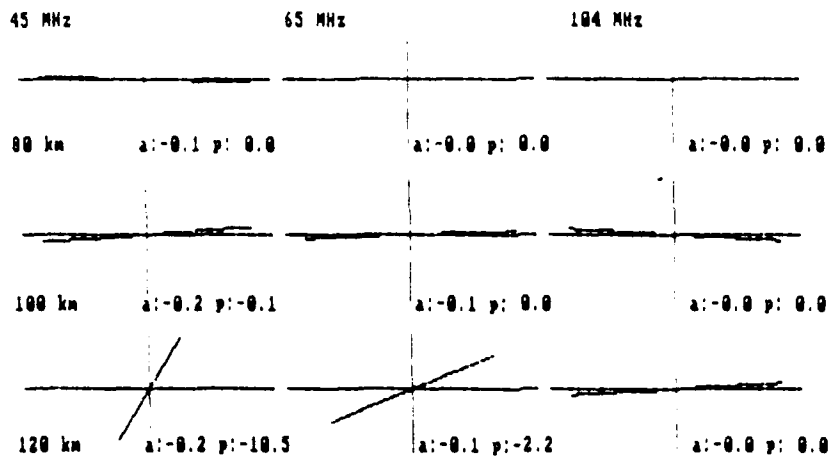
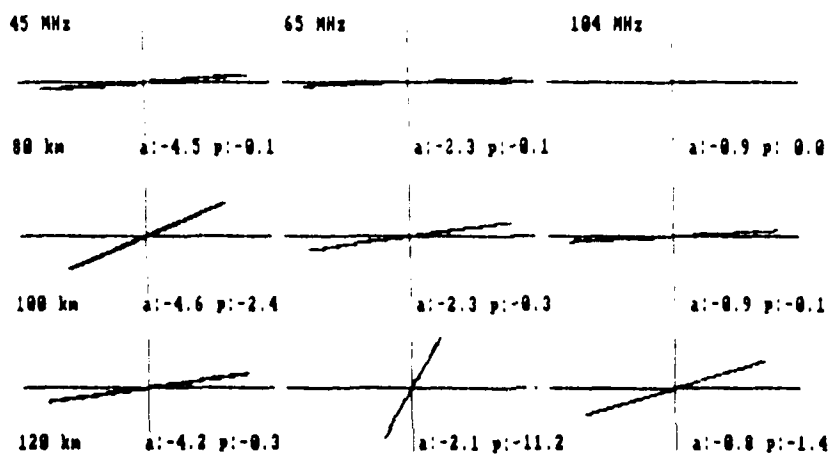


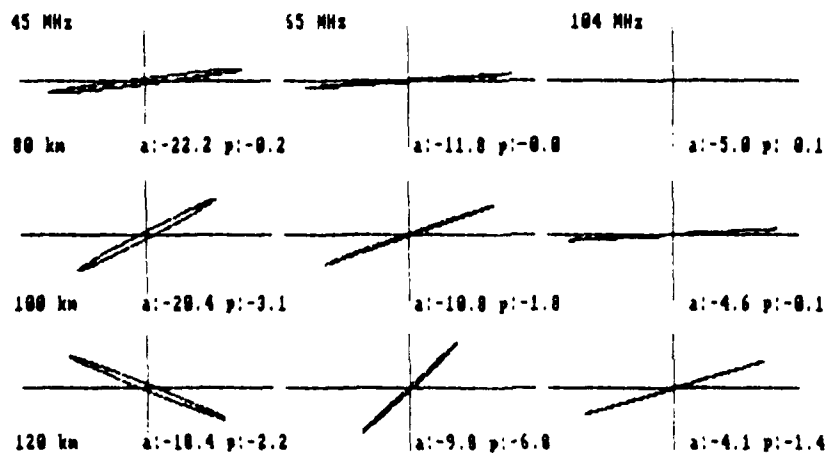
Figure 9.2. Collision frequency profile used for computation of Faraday rotation by raytracing.



A. Undisturbed ionospheric conditions.

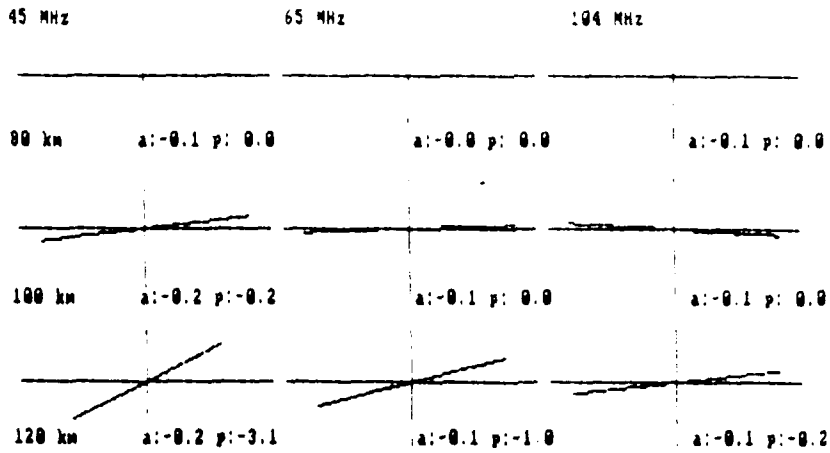


B. 2 dB vertical absorption at 30 MHz during a PCA.

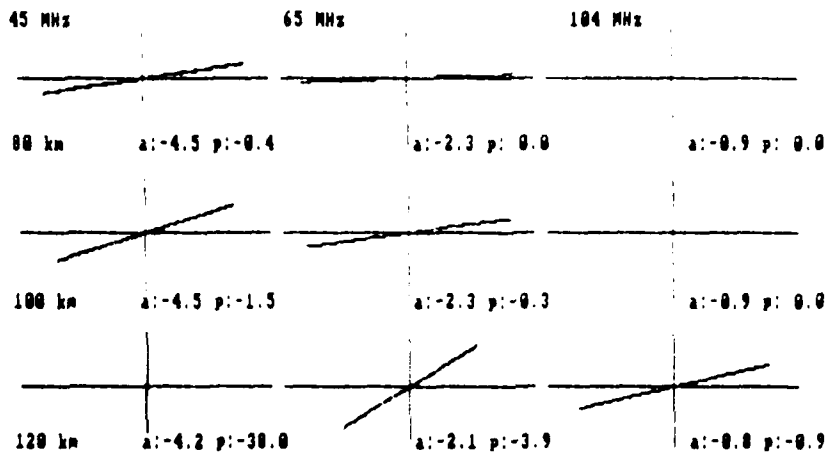


C. 7 dB vertical absorption at 30 MHz during a PCA.

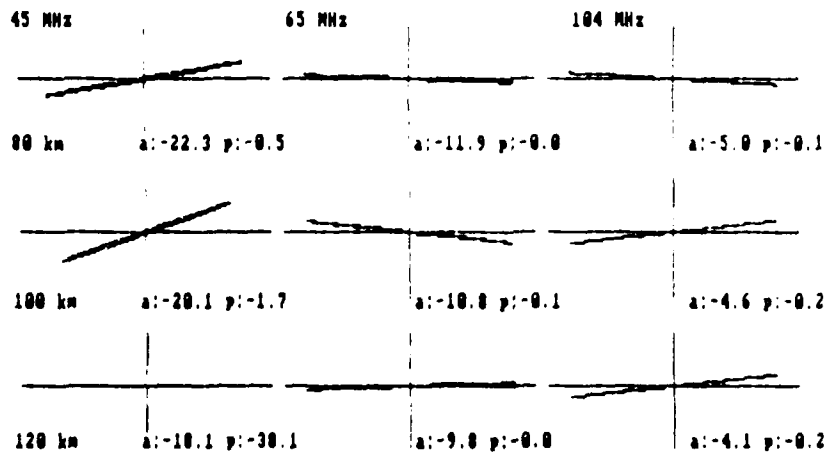
Figure 9.3. Polarization ellipses computed for the path between a transmitter at Thule AB, Greenland, to a midpath position towards Sondrestrom AB, Greenland.



A. Undisturbed ionospheric conditions.



B. 2 dB vertical absorption at 30 MHz during a PCA.



C. 7 dB vertical absorption at 30 MHz during a PCA.

Figure 9.4. Polarization ellipses computed for the path between the mid path position and a receiver at Sondrestrom AB, Greenland.

must be remembered, that the total depolarization for the meteor scatter path contains other depolarizing processes, and the numbers presented here only represent the Faraday rotation effects for the paths connecting the meteor trail with the transmitter and receiver respectively.

It is seen that insignificant Faraday rotation is encountered below 100 km at all frequencies during undisturbed ionospheric conditions. Larger amounts of Faraday rotation are present at 120 km and severe mismatch is possible for trails in the height range between 100 and 120 km at 45 MHz. Even at 65 MHz, the total Faraday rotation from the uplink and downlink may create significant polarization mismatch, whereas the Faraday rotation at 104 MHz is insignificant in all cases.

During a PCA increasing amounts of Faraday rotation are created as the absorption increases. Also the eccentricity of the polarization ellipses decreases, ie. the polarization changes from linear to elliptical. The decrease in eccentricity is not very large at frequencies above 45 MHz, but computations for 30 MHz, which are not presented here show a somewhat larger deviation from linear polarization. The combined Faraday rotations from the up-link and down-link paths can create severe polarization mismatch at a horizontally polarized receiving antenna at all frequencies for trails at or above 100 km.

10. DISCUSSION OF THE RESULTS

It would have been nice, at this point to give an unambiguous answer to the questions: "Are Faraday rotation effects detrimental to the operation of meteor scatter links, and if so, what should be done to circumvent them?" The results presented above indicate that Faraday rotation effects are present, and will have influence on the performance of a meteor scatter link. However, more analysis is needed to include all depolarization mechanisms on the propagation path, and the depolarization must be evaluated and integrated over the active meteor volume before the influence of depolarization can be quantified. The active meteor volume extends from 80 km to 125 km above the earth, and covers a large part of the mutually visible sky in this height range between the stations.

The depolarization computations based on raytracing have shown that Faraday rotation under undisturbed ionospheric conditions will not create significant polarization mismatch at altitudes less than 100 km, but that some effect is seen at 120 km altitude. Clegg and Davidson have published altitude distributions of meteor trails which show (Figure 10.1) the bulk of the trails occur at altitudes less than 100 km. Certain meteor scatter returns from altitudes above 100 km may have a severe polarization mismatch at the receiving antenna, but as the bulk of the trails occur below this altitude, the overall effect on

the performance of the link will be less severe due to the altitude spreading of the trails. This is supported by Nes's measurements.

During disturbed conditions, however, significant depolarization takes place at lower altitudes and the depolarization is not merely a rotation of the plane of polarization of the linearly polarized, transmitted wave. Due to the different absorption of the characteristic waves, the polarization of the wave is elliptical. This severely complicates the analysis of the total pathloss due to depolarization, but the theory also suggests that complete polarization mismatch at the receiving antenna may be a rare occurrence, as the elliptically polarized waves will always have a component matched to the receiving antenna. The ellipticity might not be very predominant as suggested by the results presented in Figure 8.3 and Figure 8.4, and it might be that a circularly polarized receiving antenna, or a simple linear polarization scheme could overcome the decrease in meteor scatter link efficiency due to Faraday rotation during PCA's.

Further analysis is needed to understand these observations. The analysis effort should include a computer program capable of performing the integration of propagation effects over the meteor scatter volume. The program would also be a good tool for analysis of links other than the AFGL, Greenland link. In addition, an experiment which measures the signal strength and polarization of meteor scatter returns in the range 30 MHz to 150 MHz is needed to verify and interpret the results of the analysis. The experiment must be capable of unattended operation, as is the present testbed instrumentation.

Nes⁽¹⁰⁾ has shown that an experiment is fairly easily performed with a pair of crossed linearly polarized receiving antennas and a two channel receiver. Such a setup can measure both amplitude and polarization of the received meteor scatter returns in real time. An automatic receiving station using this concept will be able to collect data throughout ionospheric disturbances, such as PCA's. The data from the experiment would also be useful to assess the depolarization observed for the overdense meteor returns and sporadic E reflections during various ionospheric conditions.

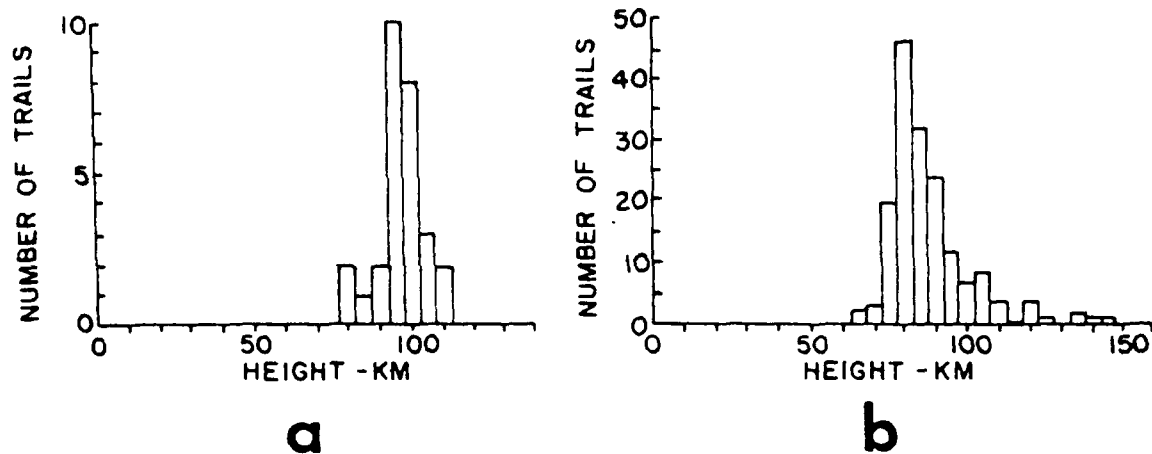


Figure 10.1. Height distribution of meteor trail scatterers. (a) represents the distribution for the Quadrantid shower, 1949 and (b) represents the distribution for daytime showers, 1949. After Clegg, Davidson.

11. EXPERIMENTAL SETUP FOR MEASUREMENT OF SIGNAL STRENGTH AND POLARIZATION

The AFGL Meteor Scatter Test Bed in Greenland consists of a transmitting station at Sondrestrom AB, and a receiving station at Thule AB. The transmitter sequentially transmits a 400 Hz FM modulated carrier at the frequencies 35, 45, 65, 85, 104, 147 MHz. The bandwidth of the transmissions are 4 kHz. The Test Bed receiver measures the characteristics of the meteor scatter returns and signals carried by other modes of propagation, which originate from the transmitter in Sondrestrom. A detailed description of the Test Bed is found in Ref. 13.

The Test Bed is currently being enhanced to perform measurements of both signal strength and polarization at all six frequencies, as opposed to the earlier measurements of signal strength only at 45, 65, and 104 MHz. The frequency coverage has been expanded to examine absorption and depolarization both at the very low end of the VHF frequency band, where Meteor scatter links have maximum yield during undisturbed ionospheric conditions, to 150 MHz where very little meteor scatter activity takes place, but where absorption and depolarization is expected to be much less severe than at lower frequencies.

The new receiving system contains a RF section and a data handling section. The configuration of the system is found in Figure 11.1. All the RF components are situated on the antenna tower along with a set of 5 element, crossed Yagi antennas, one for each frequency. The antennas are all located 1.5 wavelength above the ground. At 147 MHz, 13 element crossed Yagi antennas are used, as a higher antenna gain is needed to observe meteor scatter activity at this frequency.

Separate coaxial cables, each three wavelengths long, link each antenna to the receiver, which is mounted on the tower as close as possible to the highest frequency antennas.

The receiver has two identical RF-IF-amplitude detector channels at each frequency, thus the amplitude and phase ratio between the signals received by two crossed antennas can be measured. The polarization factor P as well as the amplitudes of the horizontally and the vertically polarized signals can be obtained.

The receiver is contained in a screened and thermostatically controlled box which is 37 X 16 X 10 cm. The receiver is connected to the data handling system through a screened multiwire telephone cable. Six data lines containing the detected signal amplitudes from two synchronous detectors, the in-phase and quadrature components, the FM detector output from one channel and a trigger signal indicating the presence of the 400 Hz FM modulation of the transmitted signals, are used to transfer data from the receiver to the data handling system. Four control lines are used to select the frequency of operation and to turn on the built-in calibration generator. 24 V AC is used to heat the receiver enclosure, and the +/-15 V DC needed for the receiver circuits is derived from the 24 V supply.

This receiver concept eliminates the need for antenna preamplifiers and long coaxial cables from the antenna tower to the receiver building, thereby reducing the EMI sensitivity of the receiving system. Also, the receiver is removed from the data handling equipment and its associated interference.

The detectors in the new receivers are synchronous detectors, which are inherently linear. This eliminates the need for involved daily calibrations. A simple, one point calibration performed with a built in signal generator is sufficient to track the accuracy of the receiver. Consequently, the need for a synthesizer to calibrate the system is eliminated.

12. DESCRIPTION OF THE RECEIVER

This section describes the overall function of the new receiver, a functional schematic of which is shown in Figure 12.1, and a picture in Figure 12.2.

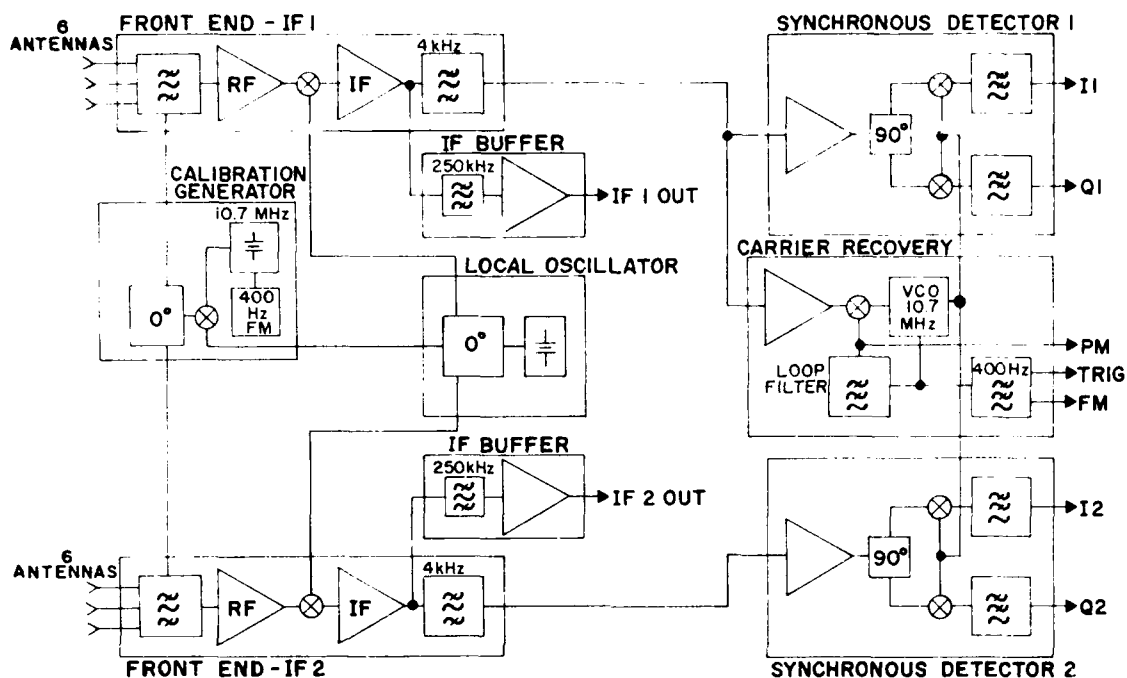


Figure 12.1. Functional schematic of the new receiver.

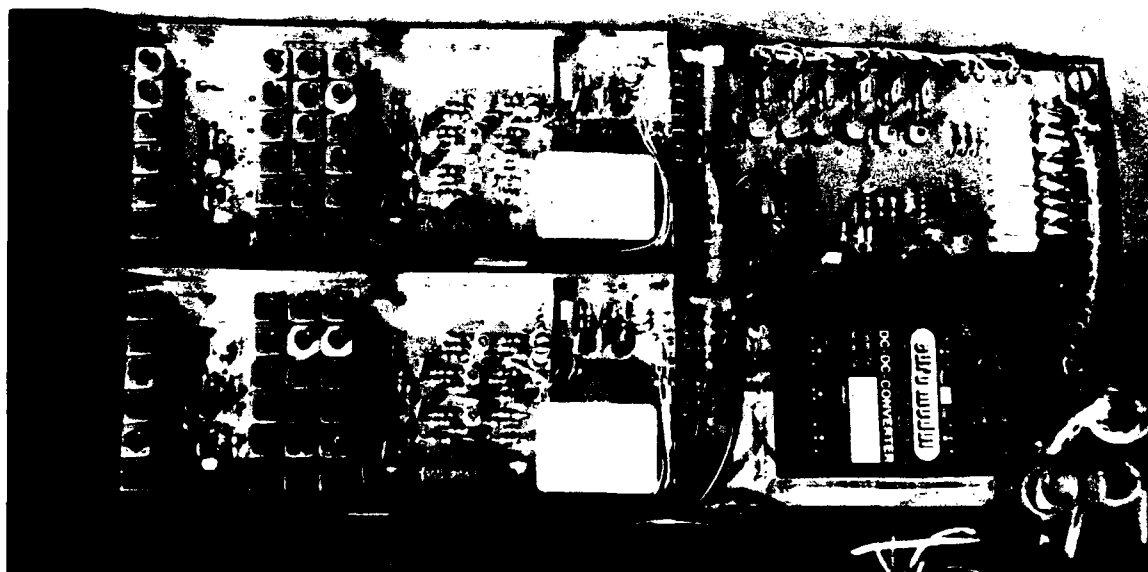


Figure 12.2. New receiver layout (Top PC board).

The receiver has two identical front-end, IF modules. The signals from the antennas are fed to a bank of image rejection filters, one filter for each receiving frequency. The order of the filters is 4, to obtain an image rejection better than 60 dB. The filter losses are distributed with one resonator in front of the first RF amplifier which defines the overall noise figure, and three resonators between the first and second RF amplifier. The amplified signals are fed to a diode mixer, and are converted to an IF frequency of 10.7 MHz. A three stage IF amplifier follows the mixer. The amplifier is constructed with transistors, and the stage gain is determined by feedback resistors, to ensure high gain stability. A ceramic IF filter with a 250 KHz bandwidth is placed between the first and the second amplifier stage. The selectivity of the receiver is determined by a crystal filter, with a bandwidth of 4 KHz, which follows the third IF stage. A second IF output amplifier with a bandwidth of 250 KHz is provided. The output is available externally on the receiver, and is intended for future specialized detectors. The module has a gain of 70 dB and a noise figure of 2 dB. The front end IF modules are mounted in shielded boxes to reduce interference from other receiver circuits.

The local oscillator module contains six crystal controlled oscillators, one for each frequency. The oscillators are emitter coupled dual transistor circuits for overtone crystals. A buffer stage amplifies the oscillator signals and delivers two identical in-phase signals for the two front end IF modules. The oscillators and the buffer are built on a PCB which is mounted in a shielded box. The oscillator is not oven stabilized as the whole receiver enclosure is thermostatically controlled to obtain stability for all circuits, and to enable operation regardless of the ambient temperature variations in the Arctic.

The output signals from the front-end IF modules are fed to two synchronous detectors. Each detector contains a quadrature phase power splitter which divides the signals into two orthogonal components of equal magnitude. These components are converted to DC voltages by a locally generated 10.7 MHz carrier which is locked to the IF signal in one of the IF channels. The obtained In-phase and Quadrature baseband signals V_I and V_Q are passed through a pair of sixth order, low pass filters with a -3 dB frequency of 50 Hz. The amplitude A of the detected signal is then:

$$A = (V_I^2 + V_Q^2)$$

and the phase angle, PH relative to the phase of the local 10.7 MHz carrier is:

$$PH = \arctan(V_Q/V_I)$$

The amplitude - phase relationships between the two IF channels are obtained from the two synchronous detectors as:

$$A_2/A_1$$

and $PH_2 - PH_1$

from which the polarization P of the received wave can be determined if two orthogonally polarized antennas are used; or the direction finding bearing can be determined if two copolar antennas are used.

The carrier recovery and FM detector circuit contains a 10.7 MHz crystal controlled VCO, which is phase locked to the IF signal from the horizontal IF channel. The IF signal is fed through a limiter amplifier with a limiting range of 80 dB to obtain a constant amplitude input signal to the phase locked loop. The loop is of second order, with a loop bandwidth of 1000 Hz. This means that the loop will track whatever angle modulation is present on the IF signal up to approximately 1000 Hz. Thus the 400 Hz FM modulation present on the received signals will be present on the control voltage to the VCO, and the control voltage can be used as a FM detector output. The VCO will also be modulated with the 400 Hz signal synchronously with the modulation of the IF signal. Consequently, this will eliminate any 400 Hz modulation component on the I and Q output voltages from the synchronous detectors. This is very desirable, as it enables the I and Q voltages to be sampled at a rate less than 800 samples per second if a 400 Hz component was present in the demodulated signal.

Usually phase locked receivers contain special circuits to speed up the acquisition of phase lock. This is not necessary for the present receiver. The incoming signal is swept across a major part of the IF bandwidth by the FM modulation and the loop bandwidth is large (1000 Hz). Consequently, lock will always be acquired in less than one frequency sweep of 1/400 sec. or 2.5 msec.

A tone decoder set for 400 Hz is attached to the FM detector output to provide a means to detect the presence of a valid RF signal from the antennas. The outputs from the tone decoder are a 400 Hz square wave signal, and a 5 V DC level signal whenever a 400 Hz signal is detected. The detector responds to frequencies in the interval 400 Hz +/- 10 Hz within 30 to 40 ms.

A means of keeping track of the calibration accuracy of the receiver during operation is needed. The receiver is fundamentally a linear device and the determination of the gain and the unavoidable amplitude and phase offsets between the

channels can be determined in the lab. Aging effects and equipment failures must be monitored daily during operation. Due to the linearity of the receiver this can be accomplished by using a calibration signal with a fixed level at each receiver frequency. The level need not be known accurately, as long as it is stable. Such signals can be obtained by mixing the local oscillator signal with the internally generated 10.7 MHz signal. Both oscillators are amplitude limited circuits, the signal amplitudes are primarily determined by the DC supply voltage. The calibration signal generator provides the signals and the receivers' responses to the signals are measured at suitable intervals. The amplitude - phase relationships at the output of the detectors can then be compared with previous measurements to generate a diagnostics message in case of failures, or a Operations Normal message in case of unchanged performance.

The level of the calibration signals must be large enough to prevent distortion of the measurement by noise from the antennas, and to verify the dynamic range of the detector. A signal with a level equal to the strongest signals received during operation is selected. The calibration generator circuit is completely shut off during normal operation in order to not generate unwanted signals at the receiver frequencies.

13. DESCRIPTION OF THE ANTENNAS

The antenna system to be used for the polarization measurement is composed of two antennas, each matched to receive one of two orthogonal polarizations, the measurement of which completely describes the polarization of an incident wave. The two antennas must have their phase centers located as close as possible to each other to avoid measurement errors due to directional effects. Usually, a pair of crossed Yagi antennas, ie. linearly polarized antennas for horizontal and vertical polarization are used and such a combination was also chosen for the present experiment. The Yagis are mounted at right angles to each other on the same boom. Corresponding elements of the Yagis are displaced as little as possible relative to each other to keep the phase centers of the antennas as close as possible.

A number of observations have been made throughout the process of selecting a suitable antenna system. Commercially available, five element Yagi antennas, fed through a gamma match were obtained and mounted orthogonally on the same boom. The polarization purity of the resulting antenna system was not at all satisfactory. Both antennas responded with maximum received signal level to a linearly polarized signal approximately 45 degrees off the axis of the individual Yagis. Also, it was noted that the isolation between the antennas, when one was used for transmitting and the other for receiving was only 4 - 8 dB. Finally,

the tuning of the gamma match on one antenna had a strong influence on the tuning of the gamma match on the other antenna.

The problem has been analyzed and it has been found that a balanced feed system will reduce the coupling between the antennas and provide isolation exceeding 30 dB. Two different antenna systems have been tested. One was composed from two commercially available, five element Yagis mounted on the same boom. The parasitic elements are mounted on the side of the boom so that the antenna system is not totally symmetric with respect to the center of the boom. The feed elements have been modified to be folded dipoles fed through a 1:4 impedance step up, broadband balun and a tuning network.

The other antenna system consists of two six element Yagis mounted through the same boom. The feed elements are center fed dipoles coupled to the coaxial feed lines through a 1:1 impedance broad band balun. This antenna is thus completely symmetrical with respect to the boom.

The design of the folded dipole feed elements require some comments. The basic Yagi antennas, ie. the lengths and positions of the parasitic elements have been designed for desired gain and radiation pattern properties. Changing the feed element from a gamma matched dipole to a folded dipole will not change the gain and directivity of the antenna. The feed impedance of a folded dipole with equal size elements in free space is close to 300 Ohms. However, when the dipole is mounted in the Yagi array the feed impedance will be changed, usually lowered, and some reactance will be present at the design frequency. Thus, the feed impedance of the folded dipole with equal size elements can be expected to be less than the desired 200 Ohms, which is easily matched to a 50 Ohm coaxial feed line with a 1:4 impedance step up balun.

The feed impedance can be changed by using different diameter elements in the folded dipole. Feeding the folded dipole in the center of the larger diameter element lowers the impedance, and feeding the dipole in the center of the smaller diameter element increases the impedance. The folded dipoles for the five element Yagi antennas have been designed with a impedance 6 times greater than the impedance of a center fed dipole. The resulting feed impedance seen through a broadband balun with a 1:4 impedance step up ratio is approximately $50+j50$ Ohms. The reactance is tuned out with series capacitance. The required capacitance can either be placed in series with the folded dipole, equally distributed on both sides of the feedpoint, or it can be placed in series with the center conductor of the coaxial feed line. The return losses and the isolation for the 104 MHz antenna system constructed from commercially available Yagi antennas, mounted 1.5 wavelengths above the ground are shown in Figure 13.1 and Figure 13.2.

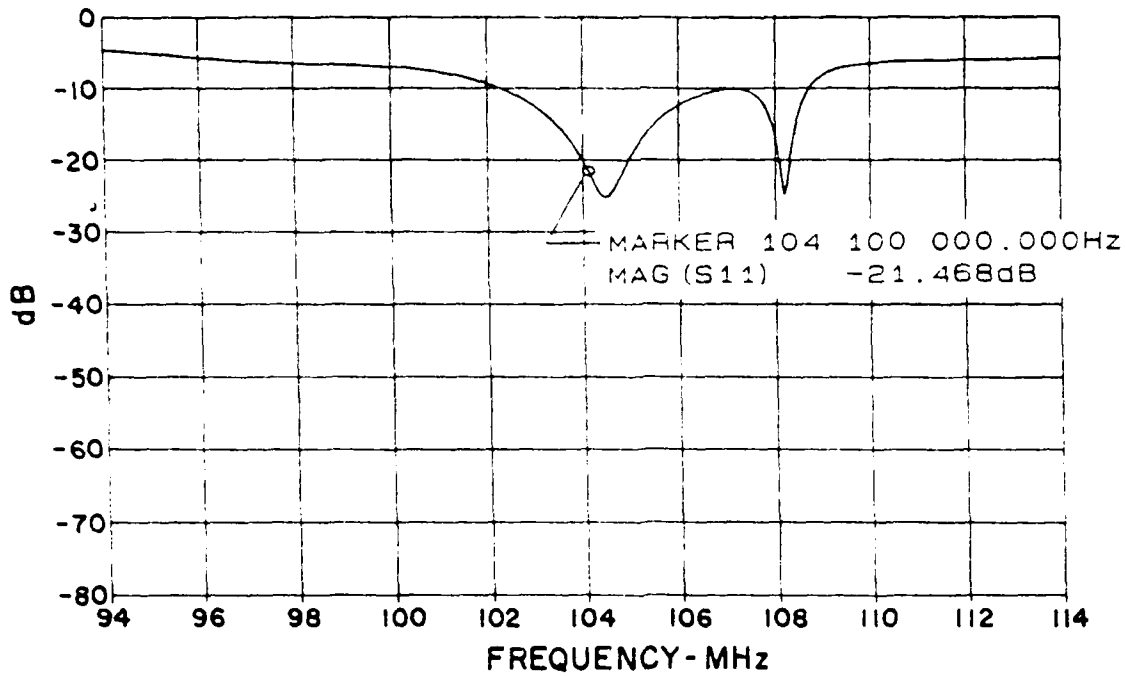


Figure 13.1. Return losses of 5 element crossed Yagi antenna at 104 MHz.

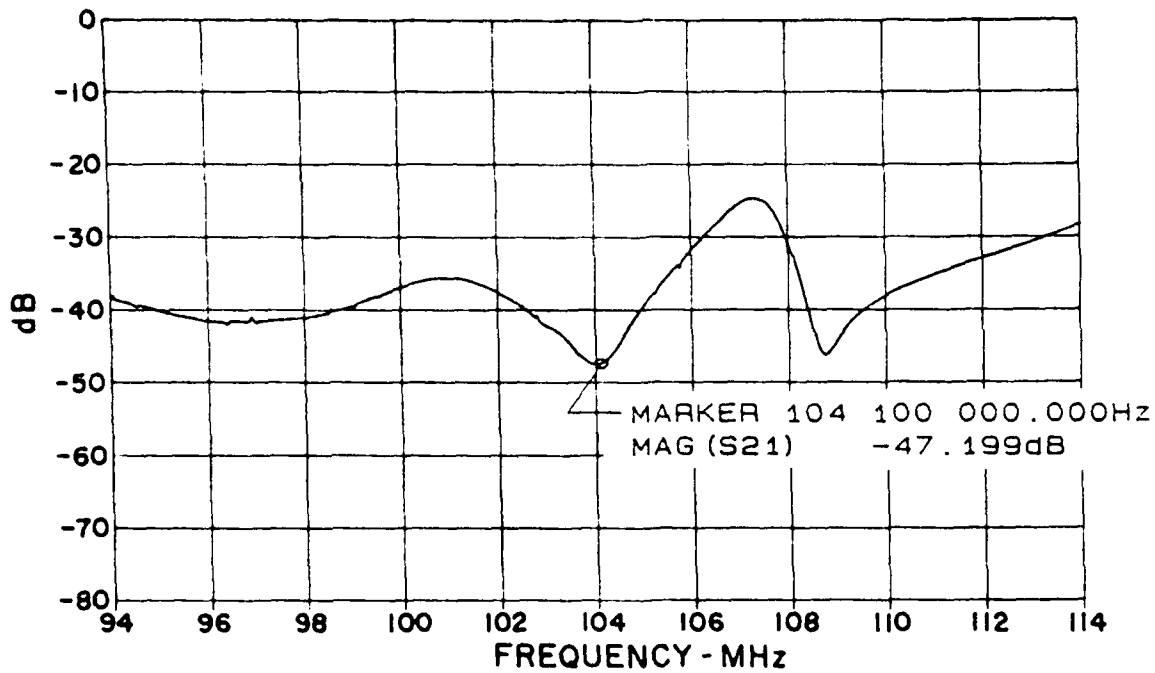


Figure 13.2 Isolation between a set of 5 element crossed Yagi antennas at 104 MHz.

The feed impedances measured for the six element crossed Yagis are approximately $40 + j30$ Ohms, which are easily matched to a 50 Ohms coaxial feed line with a 1:1 balun. The reactance part of the feed impedance is removed with a suitable capacitor in series with the center lead of the coaxial feed line. The return losses and the isolation obtained for the six element antenna system is illustrated in Figure 13.3 and Figure 13.4. It is seen from Figure 13.2 and Figure 13.4 that the off-center mounting of the parasitic elements on the five element antennas does not degrade the isolation between the antennas. Suitable antennas can therefore be constructed from commercially available antenna parts, as long as a balanced feed system is used.

The isolation between the antennas is an indication of the polarization purity of the antenna system, but the actual polarization purity of the antenna system must still be measured with a rotatable linearly polarized test antenna used for transmitting, while the crossed Yagi antenna system is used for receiving. Such tests have been performed with the five element crossed Yagis at 104 MHz, and the results are shown in Figure 13.5. It is seen that the polarization of the individual Yagis in the crossed Yagi antenna system is as expected. The horizontal Yagi yields a maximum received signal level for horizontally polarized waves, and a minimum signal level for vertically polarized waves. The converse is true for the vertical Yagi in the crossed Yagi antenna system.

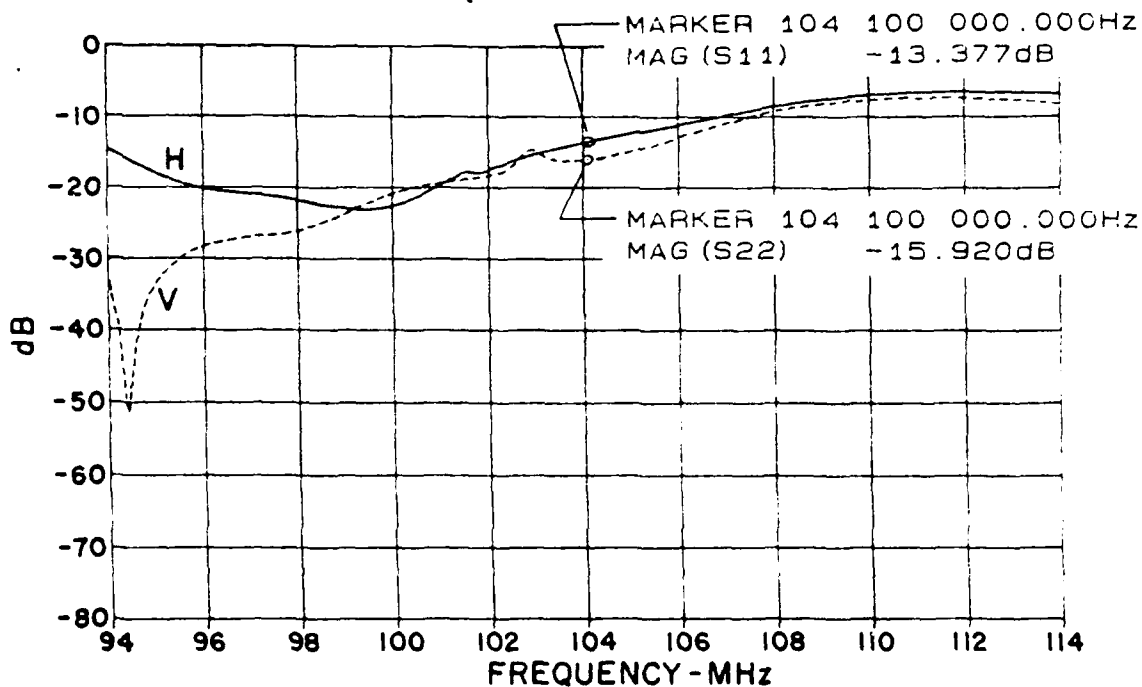


Figure 13.3. Return losses for a set of six element crossed Yagi antennas. H and V denotes the Horizontal and Vertical antennas respectively.

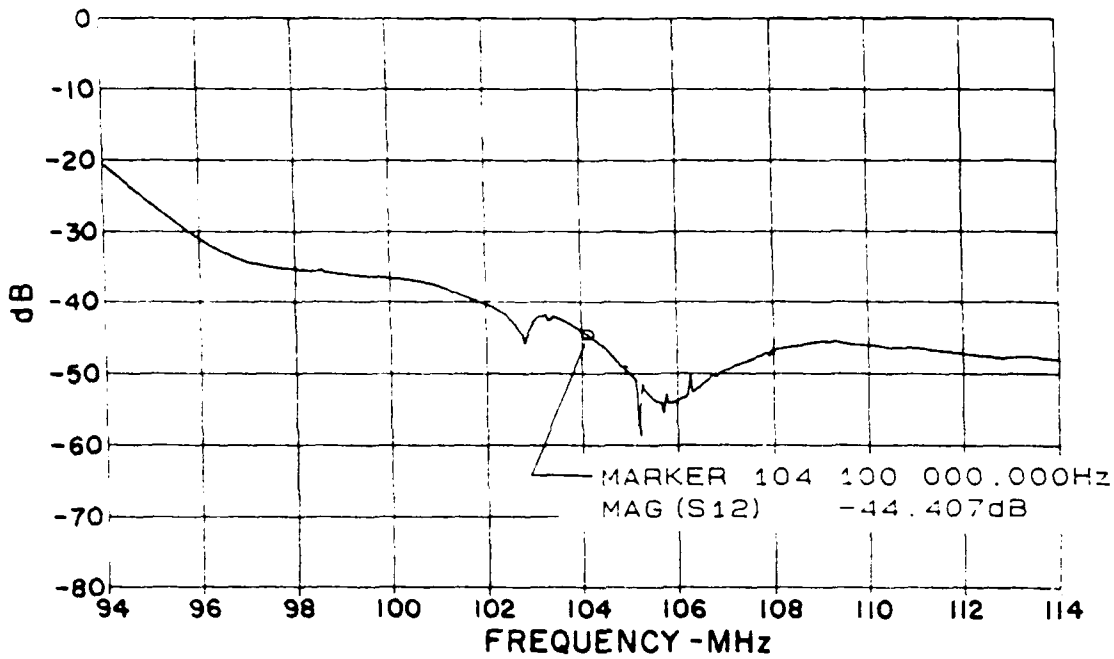


Figure 13.4. Isolation between a set of crossed, six element Yagis at 104 MHz.

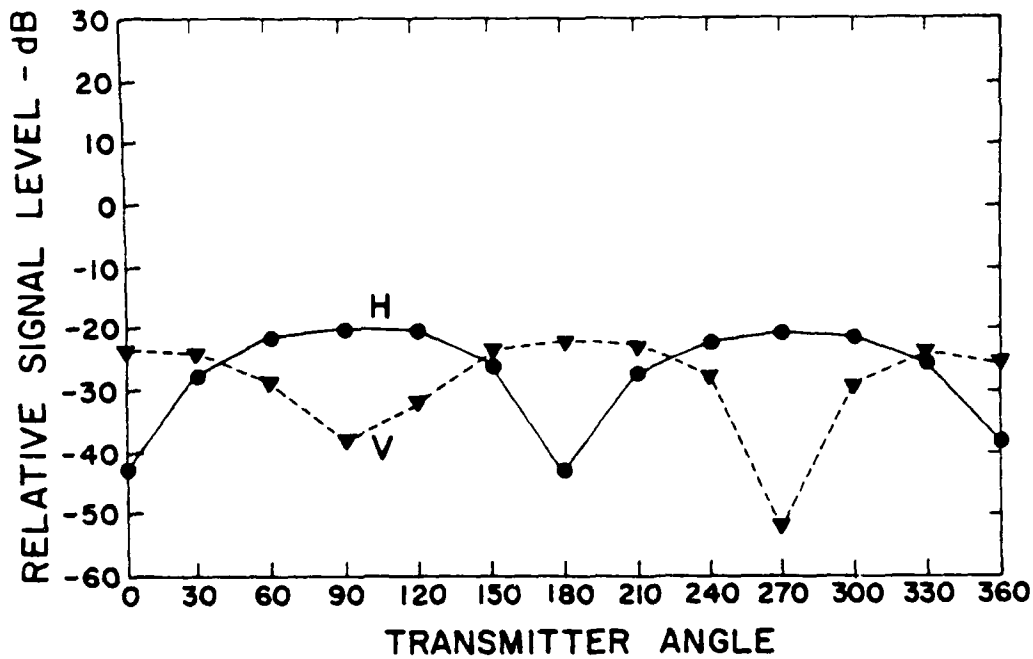


Figure 13.5. Polarization purity of a set of five element crossed Yagis. H and V denotes the response to a linearly polarized test signal versus the angle of the transmitting antenna, of the Horizontal and the Vertical antenna, respectively.

14. ASSESSMENT OF MEASUREMENT CAPABILITY AND ACCURACY

This section examines the measurement capability and accuracy of the dual polarized receiving system. The quantities to be measured are identified, and their sensitivity to the finite accuracy of the receiving system is evaluated. Then, the accuracies obtainable with the receiving system are presented for each of the measurements.

The receiver is intended for the measurement of the amplitude and polarization of the received meteor scatter signals, and the level of the background noise. The power levels are referenced to the output port of the antennas.

The polarization is represented by the complex polarization factor p , from which the polarization ellipse and the reception efficiency for a given antenna can be derived:

$$p = E_v/E_h \exp(i(\arg(v) - \arg(h)))$$

Where E_v and E_h are the amplitudes of the vertical and horizontal signals respectively, and $\theta = \arg(v) - \arg(h)$ is the phase difference between the vertical and the horizontal signals.

The sensitivity of p to variation of E_v , E_h and θ can be found by differentiation:

$$dp/p = (1/E_v)dE_v - (1/E_h)dE_h + d\theta$$

It is seen that the sensitivities to the three parameters add, and that the contributions are independent. The contributions represent the gain drift of the vertical and horizontal receiver channel and the drift of the phase difference between them.

The accuracy of the measured signal levels and of p is determined by the accuracies of E_v , E_h , and θ . These again depend on the gain and phase drift of the receiver, the signal level, the system noise level, and the isolation between the horizontal and the vertical channel of the receiving system including the antennas. Finally, the measurement is meaningless if the receiver is not locked onto a signal, and the conditions for signal acquisition are important in this respect.

The background noise is basically of galactic origin, but contributions from the receivers front end and from interference are also present. The noise is measured on the vertical antenna only. The noise does not have any coherent components relative to the detector in the receiver and the measurement presents some special problems which are discussed. The accuracy of the noise measurement is dependent on the receiver bandwidth and the gain variations.

The spectrum of the FM modulated signal transmitted by the transmitter at Sondrestrom is 4 kHz wide. The frequency deviation is 1 kHz and the modulation frequency is 400 Hz. The spectrum is shown in Fig. 14.1.

The IF bandwidth of the receiver must be equal to or exceeding the width of the transmitted spectrum. However, a much more narrow bandwidth is desirable to increase the sensitivity of the receiving systems. The FM detector is a Phase Locked Loop, which locks on to the FM modulated signal. The detector provides two outputs. One is a carrier locked to the incoming FM modulated signal, the other is a logical level, which determines the presence of the 400 Hz tone.

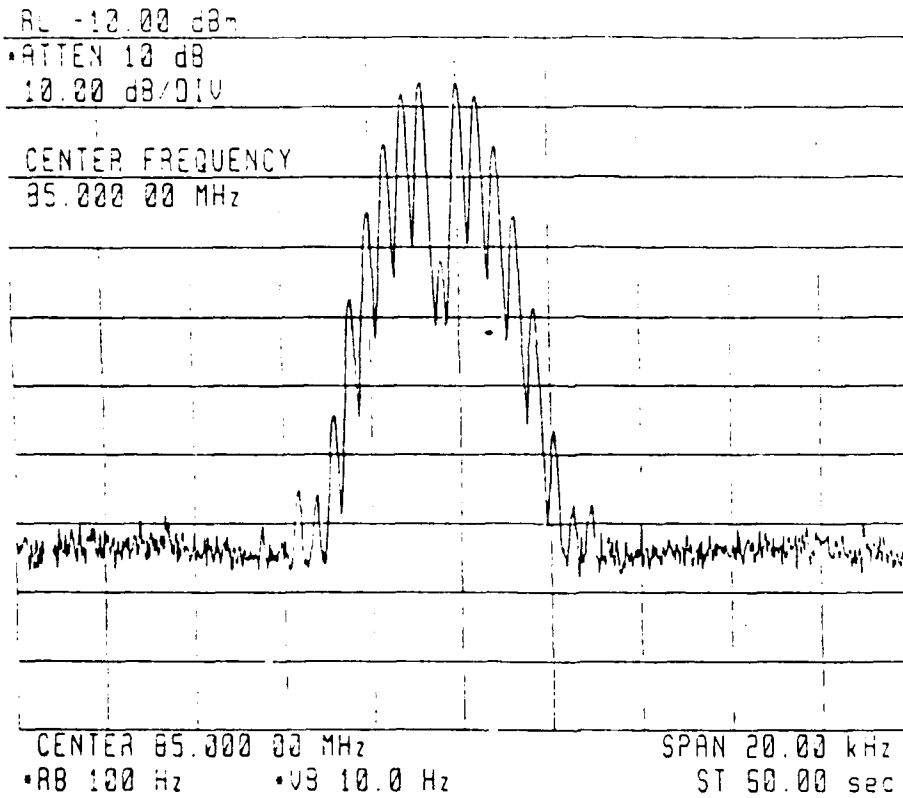


Fig. 14.1. The figure presents the spectrum of the transmitted signal. The signal is FM modulated with a 400 Hz tone and the frequency deviation was 1 kHz.

The loop bandwidth of the PLL is 1300 Hz, Fig. 14.2, and a signal to noise ratio exceeding approximately 8 dB is needed in the loop bandwidth to acquire lock.

REF LEVEL /DIV MARKER 1 008.486Hz
10.000dB 5.000dB MAG (UDF) 1.912dB

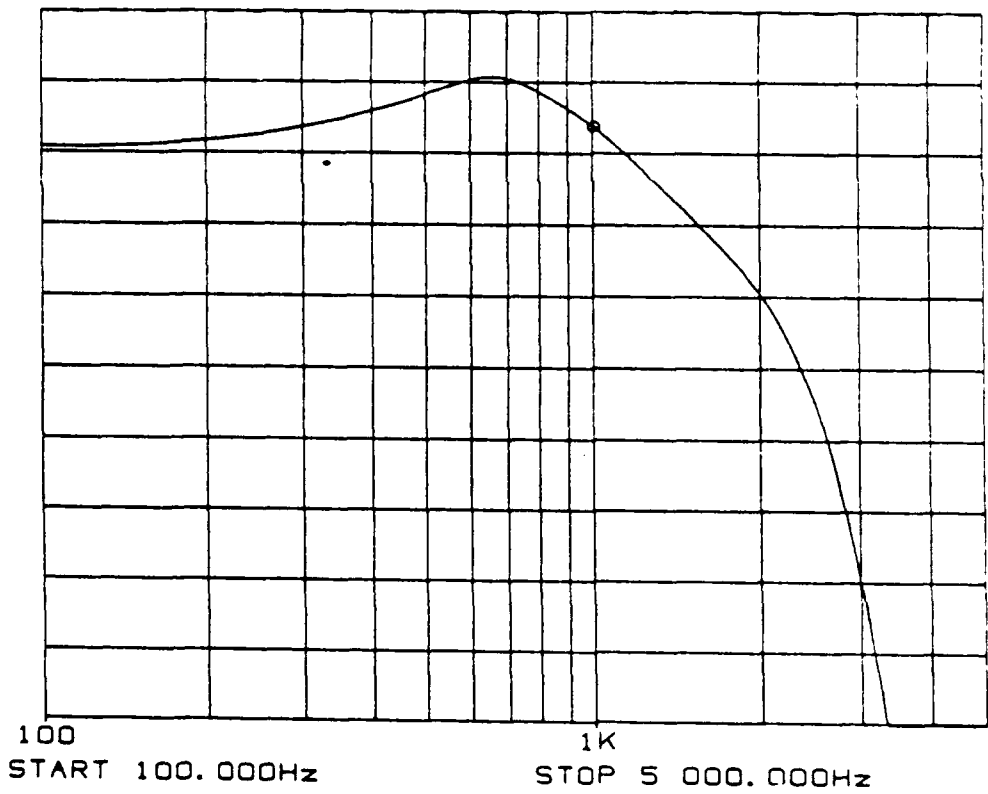


Fig. 14.2. The figure presents the loop passband of the phase locked loop FM detector.

Fig. 14.3 presents the measured acquisition level at 85 MHz as a function of the system noise level. The outputs from a signal generator and a noise generator were fed to the horizontal antenna input through a power combiner, and the output of the 400 Hz detector was monitored as an indication of acquisition. It is seen that a 3 db increase of the noise level increases the acquisition level by 3 dB.

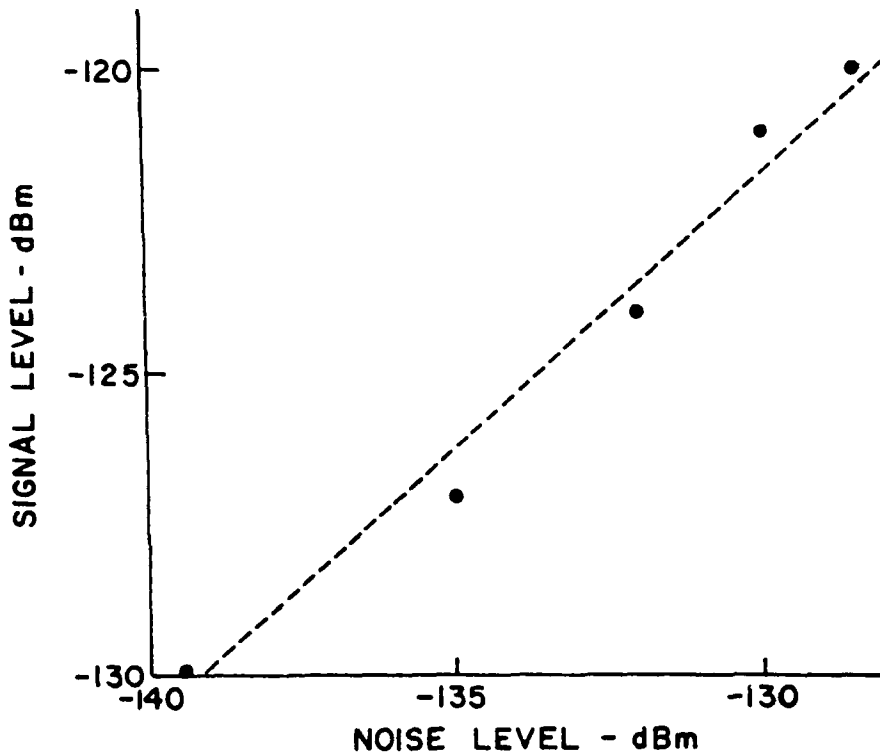


Fig. 14.3. Acquisition level as a function of the noise level at the antenna port. The measurement was performed at 85 MHz using an external signal generator and a noise source.

The ability of the receiver to capture short lived signals is dependent on the acquisition time. The FM detector has two time constants which determine the acquisition time. The received FM modulated signal sweeps across the bandwidth of the RF PLL in 2.5 msec. equivalent to 400 times a second. Thus, provided the signal to noise ratio is large enough to sustain phase lock, the acquisition time of the RF PLL is always less than 2.5 msec.

The AF PLL, ie. the 400 Hz detector has a RC time constant in the output to eliminate false lock indications. This time constant

produces an acquisition time of approximately 40 msec for the 400 Hz detector, Fig. 14.4.

Thus, the acquisition limits are: The signal to noise ratio in a 1000 Hz bandwidth must exceed 8 dB in 40 msec to obtain acquisition.

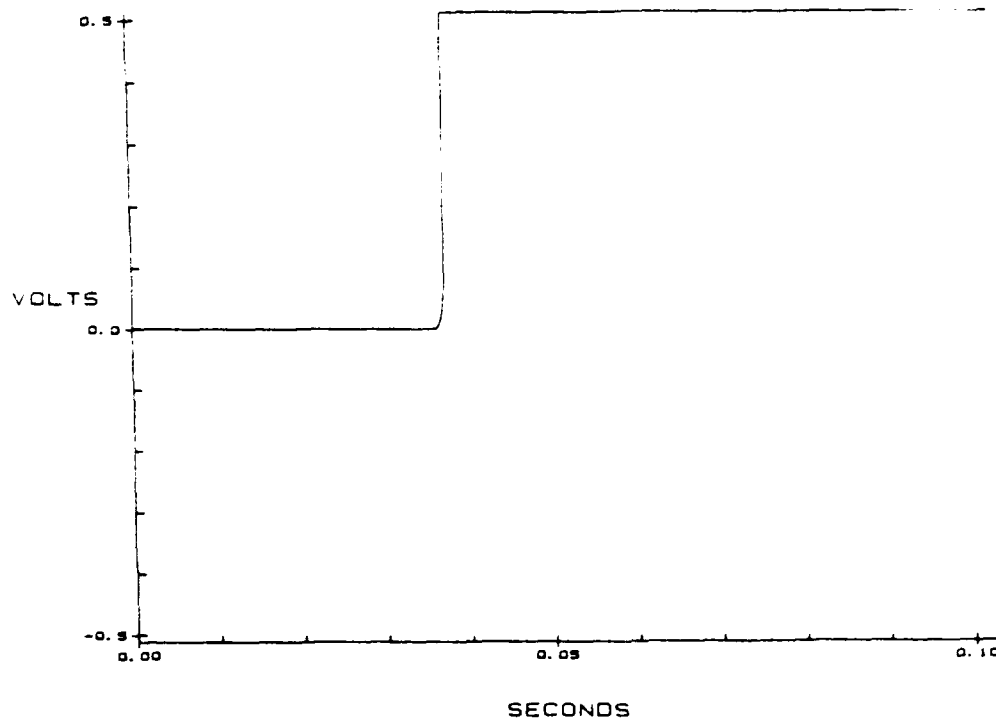


Fig. 14.4. Acquisition time of the receiver. The figure presents the acquisition flag as a function of the time after a -110 dBm signal was applied to the horizontal antenna input. The acquisition time is 40 milliseconds.

The medium term (two days) amplitude and phase accuracy has been determined with the receiver installed on the antenna tower at Thule AB, Greenland. All antennas were connected and the receiver was operated with the normal two hour cycle of operation, scanning through all six frequencies. Self calibrations were performed with the built in signal generator throughout the period, both in synchronism with the sequence and at random. The means and standard deviations of 38 successive measurements of the amplitudes and phase difference of the signal from the calibration signal generator in the receiver are presented in Table 14.1.

35 MHz Horizontal:	Mean:	-101.51 dBm.	Sdev:	0.31 dBm.
35 MHz Vertical:	Mean:	-98.59 dBm.	Sdev:	0.25 dBm.
35 MHz Angle:	Mean:	8.90 deg.	Sdev:	6.09 deg.
45 MHz Horizontal:	Mean:	-95.17 dBm.	Sdev:	0.19 dBm.
45 MHz Vertical:	Mean:	-97.37 dBm.	Sdev:	0.13 dBm.
45 MHz Angle:	Mean:	116.42 deg.	Sdev:	1.01 deg.
65 MHz Horizontal:	Mean:	-93.92 dBm.	Sdev:	0.08 dBm.
65 MHz Vertical:	Mean:	-93.68 dBm.	Sdev:	0.11 dBm.
65 MHz Angle:	Mean:	194.90 deg.	Sdev:	2.76 deg.
85 MHz Horizontal:	Mean:	-94.12 dBm.	Sdev:	0.01 dBm.
85 MHz Vertical:	Mean:	-95.09 dBm.	Sdev:	0.09 dBm.
85 MHz Angle:	Mean:	336.13 deg.	Sdev:	1.37 deg.
104 MHz Horizontal:	Mean:	-97.54 dBm.	Sdev:	0.08 dBm.
104 MHz Vertical:	Mean:	-93.02 dBm.	Sdev:	0.29 dBm.
104 MHz Angle:	Mean:	308.53 deg.	Sdev:	2.25 deg.
147 MHz Horizontal:	Mean:	-92.21 dBm.	Sdev:	0.01 dBm.
147 MHz Vertical:	Mean:	-88.63 dBm.	Sdev:	0.06 dBm.
147 MHz Angle:	Mean:	341.22 deg.	Sdev:	1.48 deg.

Table 14.1. Means and standard deviations of 38 measurements of the amplitude and phase of the built in calibration generator. The measurements were performed over a two day period.

A short discussion of the results presented in Table 14.1 is needed, as several factors might influence the measurements to mask the medium term drift, and it must be evaluated if the results represent the full drift. The temperature of the receiver had a cycle of approximately 30 minutes, and a temperature deviation of 6 deg. C. The measurements could have been performed in close synchronism with the temperature cycle, which would mask any temperature drift. The gain and phase shift of the receiver chains and the output of the calibration generator might drift in synchronism, which would mask the medium term drift. However, the measurements performed in synchronism with the two hour sequence and at random do not differ, and synchronism with the heating cycle of the receiver cannot be the reason or the small drift. The receiver chains have approximately 130 dB voltage gain from the antenna ports to the output of the synchronous detectors, whereas the calibration generator is a low gain device with a level loop. Although the measured drift represents the combined drift of the calibration generator and the receiver chains, due to the large difference in gain, it is evident that most of the drift must originate from the receiver chains.

It is of interest to note the difference between the frequencies. The very small drift at 85 MHz and 147 MHz illustrates that the

common circuits in the receiver chains: The RF and IF amplifiers, and the IF Crystal filters are very stable, and the difference in gain and phase stability must originate from the image rejection filters and associated circuits, or from slight variations of the antenna return losses.

As expected, the phase measurement has been found to be sensitive to small changes in the system configuration, whereas the amplitude measurements stay stable if small adjustments are performed on the front end filters and the antennas.

The results of the self calibrations are stored with full numerical resolution, whereas the waveform data are stored with a resolution of 0.25 dBm and 3 deg. respectively. This choice of resolution fits the accuracy of the amplitude and phase measurements.

The receiver channel isolation is measured with one channel terminated into a 50 Ohm load and the other connected to a signal source. Then a signal large enough to be measured by both channels, but small enough not to overload either of the channels is supplied to the receiver. The channel isolation has been measured to exceed 60 dB without and 35 dB with the calibration generator connected to the front ends, independent of the channel frequency. The channel isolation is thus primarily defined by the isolation in the calibration generator which is determined by the resistors in the power divider. A channel isolation of 35 dB is equivalent to a 0.03% crosscoupling, and the equivalent, but undesired polarization factor is 0.017, which is insignificant.

The Matching of the antennas, expressed as the return loss or the reflection coefficient ranges from -15 dB to -30 dB, and the isolation between the horizontal and the vertical antennas at a particular frequency ranges from 18 to 40 dB, or less than 1.6% crosscoupling. The worst case error of the measured polarization factor due to antenna crosscoupling is then 0.12. It is seen that the antenna isolation is an important parameter and that the isolation should exceed 20 dB.

The total measurement accuracies can now be discussed.

The accuracy of the signal level measured on the horizontal and the vertical antenna is the sum of the gain drift and the crosscoupling between the antennas. Of these the gain drift is dominant. The gain drift originates mainly from the front end filters and is therefore dependent on the selected frequency. The standard deviation of the drift ranges from 0.01 dB to 0.3 dB. The equivalent maximum drift of the detector output voltage, which is used to evaluate the polarization factor is 3%.

The gain drift influences both the signal and the noise measurement. In communication systems, the channel capacity is determined by the signal to noise ratio, and the gain drift is not important. However, the accuracy of the measurement of the absolute signal levels is directly influenced by the gain drift.

The drift of the phase difference between the horizontal and vertical channels is also dependent on the frequency selected. The standard deviation of the phase drift ranges from 1 to 6 degrees, the maximum being approximately 10 degrees.

The discussion of the errors induced on the determination of the polarization factor is more involved. It must be deduced from observation of the sample used to evaluate the standard deviation of the gain drift, that the drift of the vertical and horizontal channels are uncorrelated. As such the errors add up in quadrature and the combined error is 4.2%.

The worst case accuracy of p is then: $(4.2\% + i0.15 \text{ 'rad'})$; 0.15 rad represents 2.8% of the total angular span of 2π rad. The angular error is therefore of the same order of magnitude as the amplitude errors, although the number seems larger.

The worst case errors of the polarization efficiency is evaluated and contoured for two cases of receiving antennas: For a horizontal, linearly polarized antenna, and for a RHC antenna. The absolute value of p has been changed from 0 to 1 in steps of 0.1, and the angle has been incremented by 10 degrees from 0 to 180 degrees. Keeping in mind that the error in θ does not influence the combined error in the case of the linearly polarized receiving antenna, the combined errors are smaller than the errors for the RHC case. Very large errors occur for certain values of θ , and they may seem unreasonable. However the large errors occur for values of p close to LHC polarization, ie. the polarization orthogonal to the polarization of the receiving antenna. The polarization efficiency function has a singularity in this point and the error has no physical meaning.

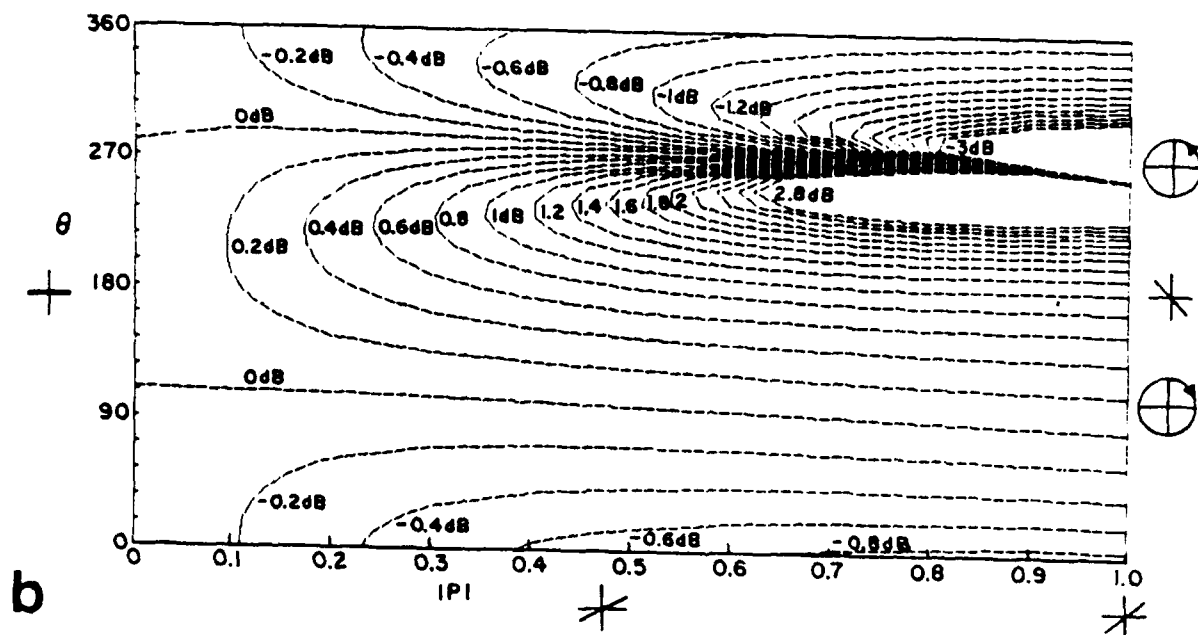
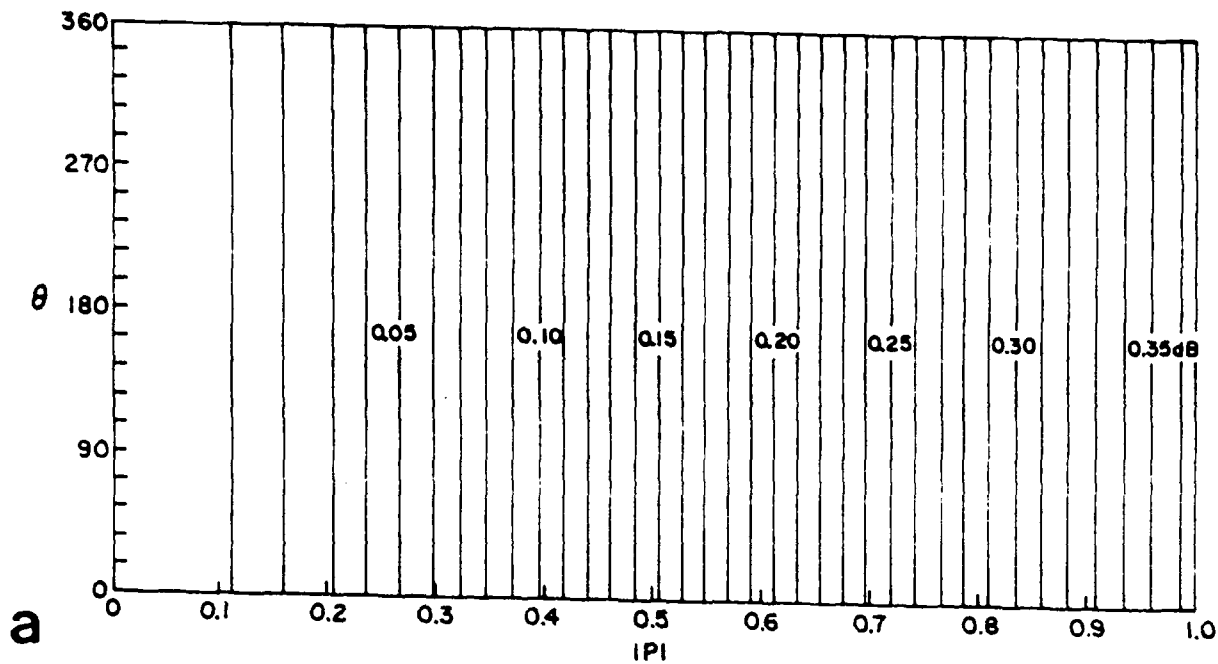


Fig. 14.5. Contour plots of the error obtained when polarization data recorded with the AFGL meteor scatter receiving facility at Thule, Greenland, are interpreted with model antennas. A: Horizontally polarized dipole. B: RHC polarized antenna.

14.6 NOISE MEASUREMENTS

The measurement of noise presents some special considerations which must be observed. These are presented below. The noise found in the receiving system originates from the receiver front end and the Galaxy. The noise is Gaussian distributed, with a frequency independent spectral density. However, the spectrum is limited by the receiver circuits and the measured noise power must be referenced to the bandwidth in which it is measured. A measure of noise which is independent of bandwidth is the noise temperature T , measured in degrees Kelvin. The relation between the noise power and the noise temperature is:

$$P = k T B;$$

where P is the noise power, T is the noise temperature, k is Boltzmanns constant $1.38E-23$, and B is the bandwidth.

Noise power or noise temperature is used at random below, with the implied understanding this relation exists between them.

The receiver is linear, which means the measurement of the noise level should not present any problems, as a bandlimited, Gaussian signal is still Gaussian at the output of the receiver. The noise power referenced to the antenna ports of the receiver can be measured as the RMS value of a number of samples of the output voltage from one of the synchronous detectors. The sampling must be performed fast enough in relation to the bandwidth of the post detection filters to preserve all spectral components of the output voltage.

The phase locked loop in the FM detector produces the oscillator signal used for the synchronous detection. During the noise measurements the PLL is unlocked and the control voltage will swing between the limits of the loop integrator due to the noise signal present on the input of the loop. As a result the oscillator frequency will also sweep a part of the IF spectrum, as the oscillator is FM modulated by the noise signal. The modulation has no amplitude component. It can be shown that provided the oscillator sweep does not exceed the IF passband, the post detection filter bandwidth is much less than the IF bandwidth, and the FM noise modulation is not correlated with the noise in the IF passband, then the detected RMS noise power is independent of the FM modulation.

These conditions are not fulfilled for the horizontal channel of the receiver, as the noise signal in the passband also drives the PLL. However, the noise in the vertical receiver channel is uncorrelated with the noise in the horizontal channel, and the vertical channel is consequently used for the noise measurements.

The noise bandwidth of the receiver is determined by the low pass filters which follow the synchronous detectors. The amplitude transfer function of the filters is shown in Fig. 14.6. The -3 dB bandwidth, which is close to the noise bandwidth of the filters is 50 Hz.

The noise voltage found in this spectrum originates from both sidebands relative to the oscillator frequency used for the detection. The noise signals present in the sidebands are not correlated, which means they add in the detection process. The noise bandwidth of the receiver as such is therefore twice the noise bandwidth of the low pass filters ie. 100 Hz.

The width of the signal spectrum after the synchronous detectors is still defined by the low pass filters, 50 Hz, and the signal can therefore be sampled with 100 samples/second without exceeding the Nyquist limit for spectrum preservation. It must however be remembered that the noise measurement, referred to the antenna terminals represent the noise power in a 100 Hz bandwidth.

REF LEVEL /DIV MARKER 63.865Hz
 20.000dB 5.000dB MAG (UDF) 15.244dB

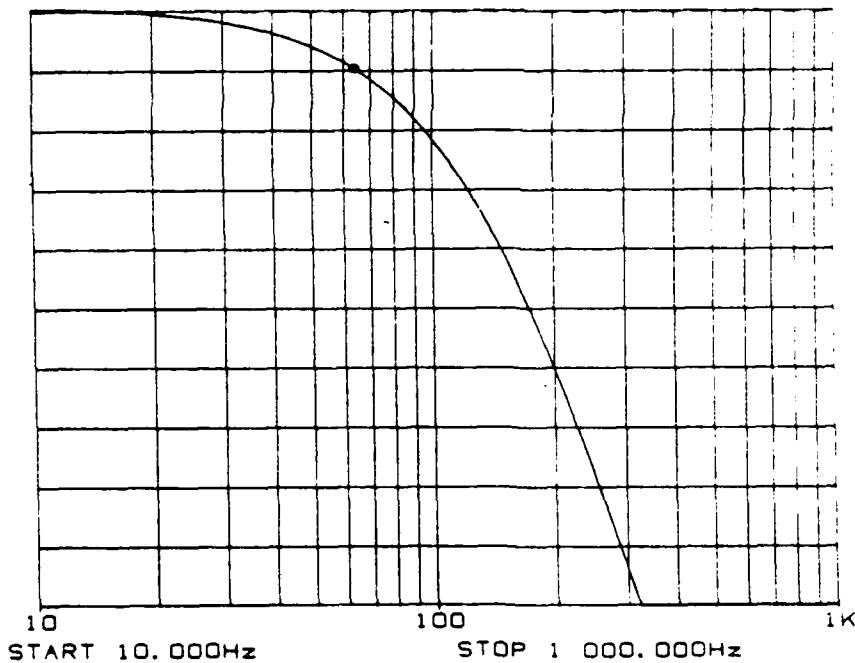


Fig. 14.6. Amplitude transfer function of the post detector filters.

The receiver, seen as an instrument for noise measurements, is a 'Total Power Radiometer'. The resolution of such an instrument, ie the closest spaced noise temperatures which can be distinguished is:

$$dT = T_{\text{sys}} / (B_w t_{\text{int}});$$

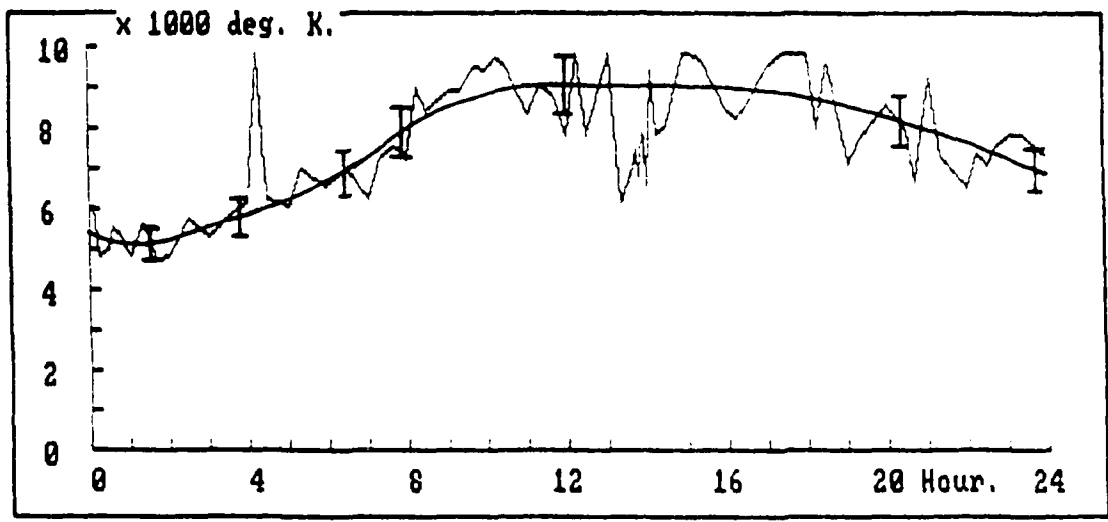
Where dT is the resolution, T_{sys} is the noise temperature, B_w is the bandwidth and t_{int} is the integration time over which the noise measurement takes place.

It is seen that a good resolution, in our case a smooth daily noise curve is obtained with large bandwidths and or large integration times.

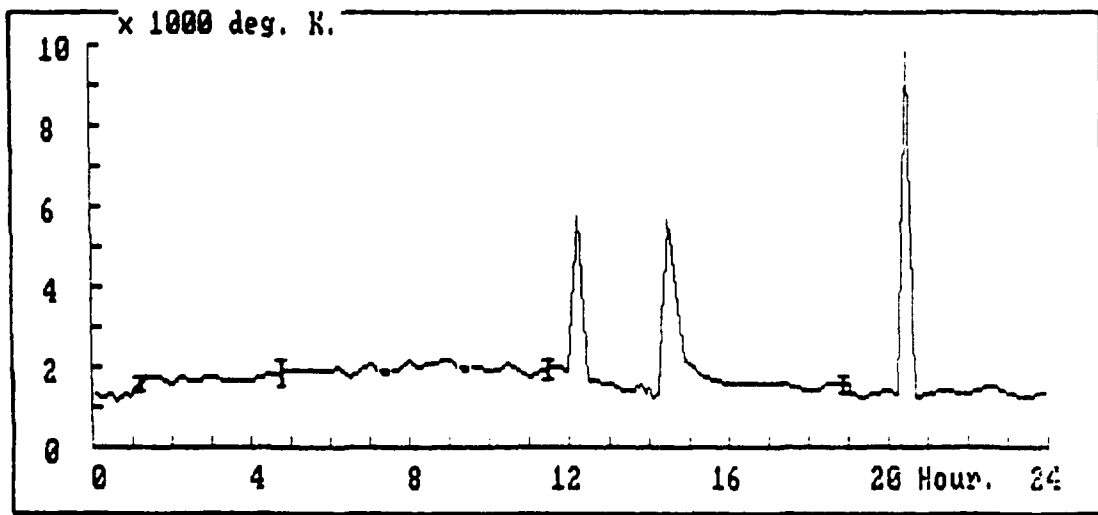
The noise measurement is performed on 500 samples of the noise voltage at the output of the synchronous detector, which represents a 5 second period of noise. The RMS value of the noise voltage is computed and referenced to the noise power at the antenna port through the gain calibration constant of the receiver. The integration time is thus 5 seconds. The bandwidth is 100 Hz as explained above, and the resulting resolution is then: $T_{\text{sys}} / \text{sqrt}(100*5)$; or 4% of T_{sys} . A larger bandwidth, for example 30 kHz, would increase the resolution to 0.3%.

To this must be added the influence of the gain variation of the receiver, which is approximately 0.2 dB. The resolution and the gain drift are statistically independent, so the combined inaccuracy of the noise measurement is approximately 7%, or 0.35 dB. The peak deviation can reach larger values and interference will when present introduce large deviations from the expected diurnal variation of the noise.

Two examples of noise measurements are shown in Fig. 14.7. The examples show the daily variation of the system noise at 35 and 85 MHz. Both records show bursts of interference, but the mean value of the noise drawn on the records agree well with the expected galactic and receiver noise. Bars indicating the expected standard deviation of the measured noise temperature have been marked on the graphs. It is seen that the calculated and measured fluctuations of the noise agree well.



Station: \$Thule; Frequency: 35MHz; Date: 24/03/1988.



Station: \$Thule; Frequency: 85MHz; Date: 24/03/1988.

Fig. 14.7. Examples of the measured diurnal variation of the system noise at 35 and 85 MHz at Thule.

15. PRELIMINARY MEASUREMENT RESULTS

A prototype of the new receiving system has been tested in the extreme North East Greenland at Station Nord (81°36'N, 16°40'W). Measurements of signal level and polarization were attempted between Sondrestrom AB and Station Nord, a distance of 1800 km, at frequencies of 45, 65, and 104 MHz during one week in April 1987. The test showed unambiguously such a long path can only be covered if very low antenna elevation angles can be exploited at both ends of the path. This is not the case for the transmitting station at Sondrestrom AB, where elevation limitations of 2 deg. in the direction towards station Nord exist. A total of four meteor trails were logged during the test, which took place during quiet ionospheric conditions. Thus, the common notion that meteor scatter propagation can be utilized on paths up to 2200 km must be questioned. The basic result of the test, which was performed with an outdoor temperature of -40 deg. C, was the concept of placing all RF components close to the antennas on the tower was feasible and does not pose any major problems.

Measurements of signal level and polarization were also conducted at 45 MHz on an approximately 1200 km East - West link between Thule AB and Station Nord throughout one week in August 1987. The test was performed just after the yearly maximum meteor activity during the Perseids shower in the second week of August. The immediate observation as the data collection process was watched was the very large duty cycle, which frequently presented itself as a almost constant signal. Many very weak and short lived returns were seen. This contrasts very much with the duty cycles of a few percent previously observed with the 1200 km Sondrestrom - Thule link. One reason for the larger duty cycle is the reduced detection bandwidth of 50 Hz, compared to the 30 kHz used in the earlier receiver. The reduced bandwidth is equivalent to an increase in transmitter power and/or antenna gain, and it is known that meteor scatter circuits in Alaska using transmitter powers of up to 10 kW into arrays of multi-element Yagi antennas exhibited very large duty cycles. This raises the question as to whether the large duty cycle is caused by many very small meteor scatter returns or ionoscatter, or both. Figure 15.1. shows an example of a five second period containing a number of weak and short lasting meteor returns.

A sequence showing classical meteor scatter returns is found in Figure 15.2. The polarization is predominantly horizontal except during fades, where the polarization becomes uncertain due to noise.

A number of sporadic-E events, characterized by a continuous, slow fading signal were observed. The events lasted up to one hour. The signals were predominantly elliptically polarized, with a tendency towards horizontal polarization. Figure 15.3. shows a sequence of sporadic-E signal. The axis of the polarization ellipse are shown for three instants during the sequence.

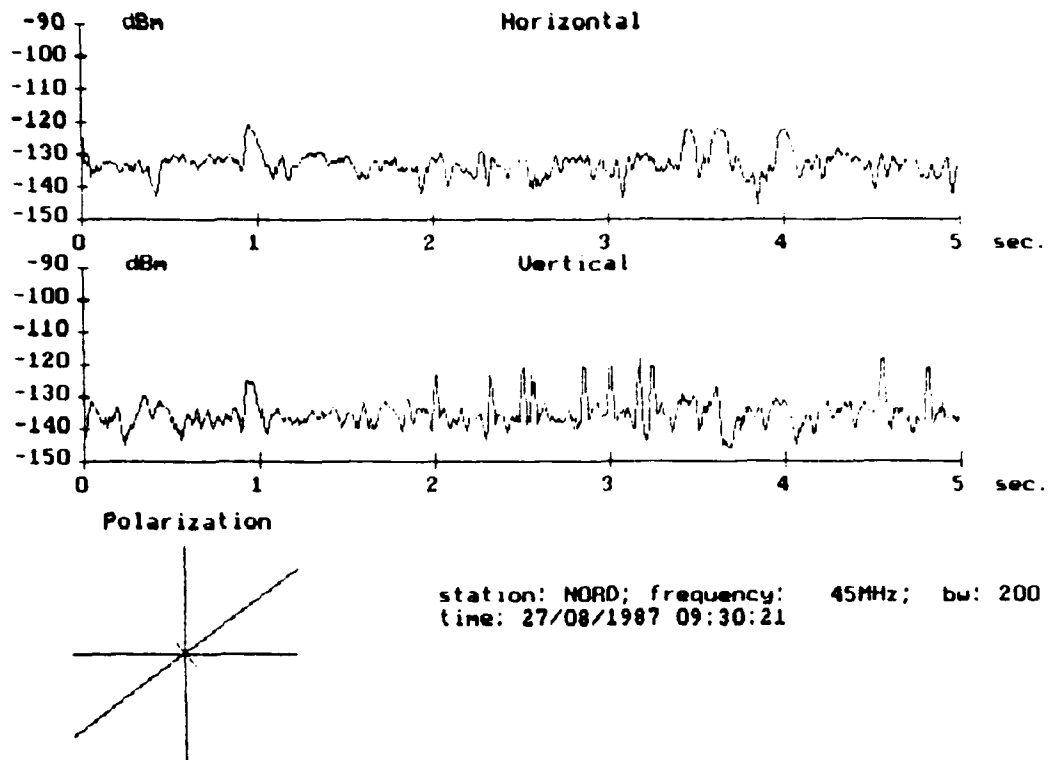


Figure 15.1. Example of a five second recording with a number of short and weak meteor scatter returns.

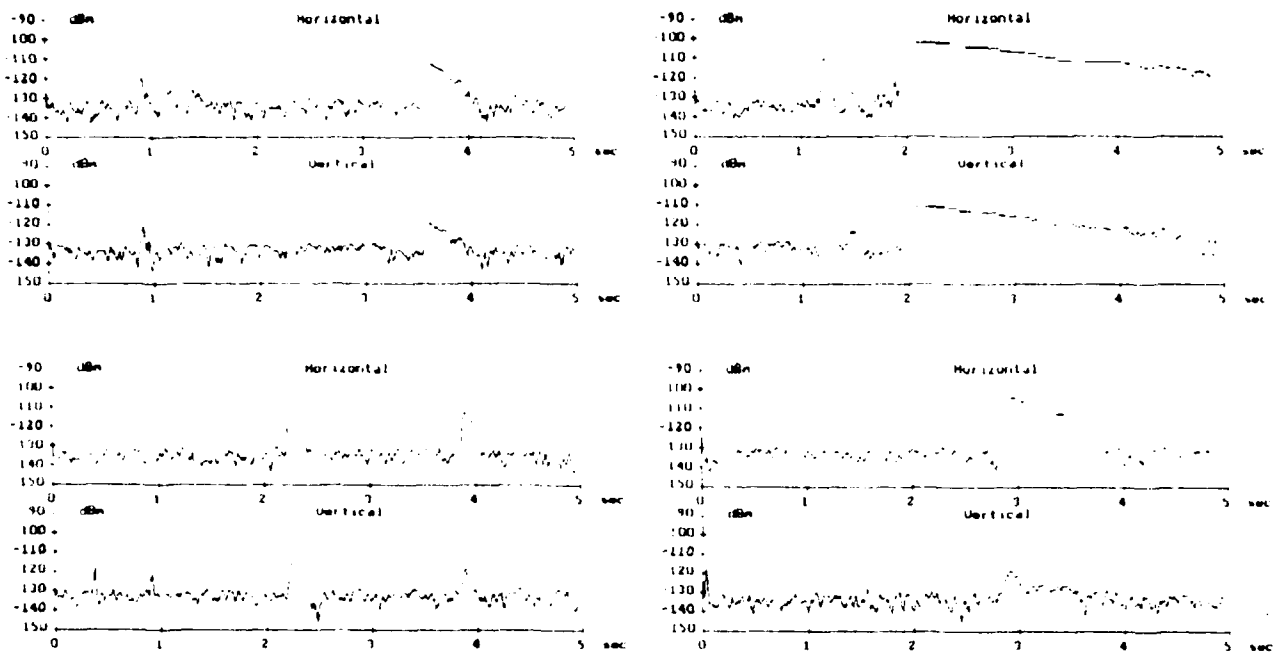


Figure 15.2. Examples of five second recordings showing classical meteor scatter returns.

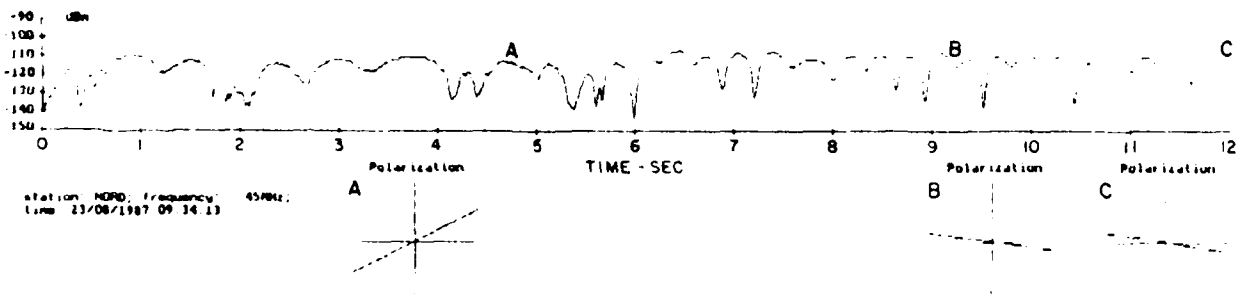


Figure 15.3. Example of a 12 second recording of sporadic-E signal. The polarization at A,B,C are shown.

16. CONCLUSIONS

A survey of the depolarization mechanisms present in meteor scatter propagation during undisturbed ionospheric conditions as well as at different levels of absorption during a PCA has been conducted. The sources of depolarization on the total propagation path for a meteor scatter link have been identified. Preliminary results of the computation of the ionospheric depolarization have been presented. The results show that Faraday rotation can create significant polarization mismatches during undisturbed ionospheric conditions if the meteor trail occurs at altitudes above 100 km and the frequency is 45 MHz or below. The bulk of the meteor trails are found below 100 km, and it is anticipated Faraday rotation will not create much degradation to the efficiency of the meteor scatter link. However, during PCA's ionospheric depolarization is present at lower altitudes and may contribute considerably to the effective pathloss for the link. A quantitative measure of this contribution is not available at this stage of the analysis, and additional analytical work is suggested to further the analysis. An experiment is currently being implemented to measure the instantaneous amplitude and polarization of meteor scatter returns in an effort to assess the depolarization effects during disturbed ionospheric conditions. The receiver and antenna system to be used for such an experiment on the AFGL Meteor Scatter Test Bed in Greenland is described. The measurement capability and accuracy of the experimental setup are discussed, providing the information necessary for analysis of the data collected by the system. Tests of a prototype of the system were performed at 45 MHz during quiet ionospheric conditions in the extreme North Greenland in April and August 1987. The operating environment ranged from -40 deg. C to + 5 deg C., and it demonstrated the concept of placing all RF components directly on the antenna tower functioned well. Examples of waveforms acquired during the tests are presented as an illustration of the capabilities of the system. A variety of meteor scatter and sporadic E signals were observed. Analysis of the data collected during the test is currently being undertaken and will be published in a following report.

For additional information on the AFGL meteor scatter program contact Mr. Alan Bailey at (617) 377-2525 or Mr. John Rasmussen at (617) 377-2109.

REFERENCES:

- 1) Beckmann, P. The depolarization of electromagnetic waves, Golem 1968.
- 2) Budden, K.G. Radiowaves in the ionosphere, University Press, Cambridge, 1961.
- 3) Davies, K. Ionospheric radio propagation, NBS monograph 80, 1965.
- 4) Ratcliffe, J.A. The magneto ionic theory and its application to the ionosphere, University Press, Cambridge, 1959.
- 5) Jones, R.M. A versatile three dimensional raytracing computer program for radio waves in the ionosphere. U.S. Dept. Commerce, 1975.
- 6) Hamberg, G. A modified version of a raytracing program for the computation of the ionospheric effect in differential doppler measurements. (in Swedish) Uppsala Ionospheric Observatory Report: UIO-SR-78-2, 1978.
- 7) Ajayi G.O. Use of a single function subroutine for multi-region ionospheric profiles with a versatile 3-dimensional raytracing program. Uppsala Ionospheric Observatory Report: UIO-SR-78-03, 1978.
- 8) Cannon, P.S.,
A.H. Dickson,
M.H. Armstrong Meteor scatter radio communication at high latitudes, AGARD CPP382, 1985.
- 9) Cannon P.S. Polarization rotation in meteor burst communication systems, Radio Science, May - June 1986.
- 10) Nes, H. Meteor burst polarization trials. IEE Electronics Letters, vol 21, no. 24, 21 November 1985.
- 11) Clegg, J.A.,
I.A. Davidson A radio echo method for the measurement of the height of the reflecting points of meteor trails. Phil. notes ser. 7, vol 41, no.312. Jan 1950.

- 12) Kossey, P.A., VLF reflection properties of the normal and
J.P. Turtle, disturbed polar ionosphere in Northern Green-
R.P. Pagliarulo, land. Radio Sci., Vol 18, no. 6, p. 907-916,
W.I. Klemetti, Nov - Dec 1983.
J.R. Rasmussen

- 13) Ostergaard, J.C., The RADC High Latitude Meteor Scatter Test
J.E. Rasmussen, Bed, RADC Report No. RADC-TR-86-74,
M.J. Sowa, July 1986. ADA180550
J.M. Quinn,
P.A. Kossey

- 14) Ostergaard. J. EC7221 Meteor Scatter Receiver manual.
ElektronikCentralen, Copenhagen. 1988.

- 15) Lawson. L. Yagi Antenna Design. The American Radio Relay
League, 1986.

- 16) Viezbicke. P.P. Yagi Antenna Design. NBS report 688. National
Bureau of Standards, Dec. 1967.

- 17) Morris. I.L. Optimization of the Yagi Array I-II. AFCRL
contract AF19(628)-2406. Oct 1964.
AFCRL-65-121, AD615742; AFCRL-65-346, AD616911

- 18) Li, Eric Receiver System Control Development for The
AFGL High Latitude Meteor Scatter Test-Bed.
(Contract NWRA-86-S-002; University of Lowell, Center
for Atmospheric Research, Lowell, MA for NorthWest
Research Associates, Inc, 300 120th Avenue Northeast,
Bldg 7, Suite 220, Bellevue, WA 98005)